Cell

ATR Mediates a Checkpoint at the Nuclear Envelope in Response to Mechanical Stress

Amit Kumar,[1] Michele Mazzanti,[2] Martin Mistrik,[3] Martin Kosar,[4,5] Galina V. Beznoussenko,[1] Alexandre A. Mironov,[1] Massimiliano Garrè,[1] Dario Parazzoli,[1] G.V. Shivashankar,[6] Giorgio Scita,[1,2] Jiri Bartek,[3,4,5,*] and Marco Foiani[1,2,*]
[1]Fondazione Istituto FIRC di Oncologia Molecolare (IFOM), Via Adamello 16, 20139 Milan, Italy
[2]Università degli Studi di Milano, 20122 Milan, Italy
[3]Institute of Molecular and Translational Medicine, Faculty of Medicine and Dentistry, Palacky University, 77115 Olomouc, Czech Republic
[4]Danish Cancer Society Research Center, 2100 Copenhagen, Denmark
[5]Institute of Molecular Genetics, v.v.i., Academy of Sciences of the Czech Republic, 14220 Prague, Czech Republic
[6]Mechanobiology Institute and Department of Biological Sciences, National University of Singapore, 117411 Singapore, Singapore
*Correspondence: jb@cancer.dk (J.B.), marco.foiani@ifom.eu (M.F.)
http://dx.doi.org/10.1016/j.cell.2014.05.046

SUMMARY

ATR controls chromosome integrity and chromatin dynamics. We have previously shown that yeast Mec1/ATR promotes chromatin detachment from the nuclear envelope to counteract aberrant topological transitions during DNA replication. Here, we provide evidence that ATR activity at the nuclear envelope responds to mechanical stress. Human ATR associates with the nuclear envelope during S phase and prophase, and both osmotic stress and mechanical stretching relocalize ATR to nuclear membranes throughout the cell cycle. The ATR-mediated mechanical response occurs within the range of physiological forces, is reversible, and is independent of DNA damage signaling. ATR-defective cells exhibit aberrant chromatin condensation and nuclear envelope breakdown. We propose that mechanical forces derived from chromosome dynamics and torsional stress on nuclear membranes activate ATR to modulate nuclear envelope plasticity and chromatin association to the nuclear envelope, thus enabling cells to cope with the mechanical strain imposed by these molecular processes.

INTRODUCTION

ATR is an essential PI3-kinase (Brown and Baltimore, 2003). Mutations in the ATR gene cause the Seckel syndrome (O'Driscoll et al., 2003), a severe disease, characterized by mental retardation, dwarfism, and defects in the DNA damage response. ATR controls several (patho)-physiologically relevant pathways (Jackson and Bartek, 2009; Matsuoka et al., 2007) and protects genome integrity by counteracting replication fork collapse (Sogo et al., 2002), fragile site expression (Casper et al., 2002; Cha and Kleckner, 2002), aberrant chromatin condensation events (Cha and Kleckner, 2002; Nghiem et al., 2001), and nuclear fragmentation (Alderton et al., 2004). Following DNA damage, replication protein A (RPA)-coated single-stranded DNA (ssDNA) nucleofilaments activate ATR (Zou and Elledge, 2003). Chromatin replication, during S phase, and chromatin condensation, during prophase, generate torsional stress at the level of the DNA fiber and DNA topoisomerases assist the replication and condensation processes to resolve the topological complexity. Unsolved topological constrains lead to highly recombinogenic and aberrant DNA transitions, DNA entangling, and breakage. In mammals, lamin-associated chromatin imposes topological impediments during chromatin replication and condensation (Bermejo et al., 2012a). The nuclear envelope (NE) is connected with the cytoskeleton (Martins et al., 2012) and is a hub for heterochromatin and late replicating chromosomal domains (Comings, 1980; Dimitrova and Gilbert, 1999; Mekhail and Moazed, 2010; Shevelyov and Nurminsky, 2012; Towbin et al., 2009). The mammalian NE has two components: the solid-elastic lamina and fluid-like membranes. The inner nucleus behaves like a compressible gel (Rowat et al., 2006) and the nucleoskeleton is 5- to 10-fold stiffer than cytoskeleton (Simon and Wilson, 2011). Being deformable, the NE is an ideal elastic structure for adsorbing and/or transducing mechanical stimuli arising inside or outside the nucleus. Chromatin dynamics generates mechanical forces that can be transmitted to the NE through the lamin-associated chromatin domains.

In yeast, when replication forks approach chromatin domains that are connected to the NE, the Mec1/ATR pathway regulates key nucleoporins to detach these chromatin regions from the NE, thus facilitating fork progression (Bermejo et al., 2011). This event prevents aberrant topological transitions that would otherwise lead to forks reversal (Sogo et al., 2002) and genome rearrangements (Bermejo et al., 2012b). However, it remained unclear how ATR senses that chromatin must be detached from the NE when forks are approaching. Moreover, does ATR

play a similar role in prophase when condensation engages chromatin domains associated to the NE? Intriguingly, it has been shown that ATR contains many HEAT repeats (Perry and Kleckner, 2003) that can behave as elastic connectors (Grinthal et al., 2010), suggesting that ATR might be influenced by mechanical forces.

We therefore investigated whether ATR responds to the mechanical stimuli deriving from chromosomal dynamics. We found that a fraction of human and mouse ATR localizes at the NE during S phase, particularly under conditions of enhanced replication stress, and in prophase of unperturbed cell cycles. Osmotic stress or mechanical stimulation of the plasma membrane cause relocalization of ATR to the inner and outer nuclear membranes, independently of the cell-cycle stage and of RPA or DNA damage. Thus, ATR responds to mechanical forces at the NE. Our observations suggest that ATR mediates a mechanical response to membrane stress that could be caused by chromatin dynamics and is important for genome integrity.

RESULTS

A Fraction of ATR Localizes at the NE

DNA torsional stress generates mechanical strain and arises during chromatin condensation, when the DNA packaging reaches the maximal complexity and, transiently, during S phase (Wang, 2002). Based on our previous findings (Bermejo et al., 2011), we reasoned that lamin-associated chromatin might mediate the transfer of mechanical forces resulting from DNA torsional stress to the NE. Given the data on ATR discussed above from our laboratories and others', we tested whether ATR localizes at the NE. We examined ATR localization by indirect immunofluorescence (IF), using an anti-ATR antibody (Ab), the specificity of which was validated in HeLa cells depleted for ATR (Figure S1A available online) and in ATR-defective human Seckel fibroblasts (Figure S1B). In asynchronous HeLa cells, ATR localized mostly in the nucleus in interphase and S phase cells (Figure 1A). In prophase, part of ATR exhibited a perinuclear distribution, which was lost later in mitosis, following NE breakdown (NEBD) (Figure 1A). Using structured illumination super resolution microscopy (SR-SIM), we analyzed ATR and Nup153 colocalization in prophase cells. Both proteins localized at the NE (Figure 1B), exhibiting 70% colocalization. Consistently, several nucleoporins, including Nup153, are targeted by ATR/Chk1 (Blasius et al., 2011; Matsuoka et al., 2007). Notably, ATR was prominently enriched at NE invaginations (Figure S1C), which often mediate the mechanical attachment of nucleoli and spindles (Beaudouin et al., 2002; Bourgeois et al., 1979). The observations described above were confirmed in primary human IMR90 and murine NIH 3T3 fibroblasts (Figure S1C). In leptomycin B (a nuclear export inhibitor; Kudo et al., 1998)-treated prophase cells, ATR intracellular distribution did not change (Figure S1D), thus arguing against a contribution of nuclear export to ATR localization. Cellular distribution of ATR was further analyzed by electron microscopy (EM). Gold ATR immunostaining revealed a nuclear and nonnuclear distribution of ATR particles (Figure 1C). A fraction of these particles localized at the NE, particularly in prophase. Indeed, whereas in interphase, among the ATR particles visible in the nucleus, 90.5% ± 3% were in the nucleoplasm and 9.5% ± 3% were at the NE, in prophase cells, 78.4% ± 3.3% were in the nucleoplasm and 21.6% ± 3.4% were at the NE.

Because ATR and Chk1 have been found associated with centrosomes (Krämer et al., 2004; Zhang et al., 2007a), we costained prophase cells with Abs against ATR and α-tubulin (Figure 2A). The ATR fraction associated with centrosomes was lower compared to the one bound to the NE and partially overlapped in places in which centrosomes contact NE. Colcemid (a microtubule-depolymerizing drug) treatment, did not affect ATR-NE association (Figure 2A). Hence, the NE-bound ATR in prophase unlikely depends on centrosomes and microtubule polymerization.

Next, we examined whether the NE distribution of ATR depended on its kinase activity and whether other checkpoint factors exhibited a similar localization. We did not observe changes in the NE distribution of ATR following treatment with an ATR inhibitor (ATRi) (Toledo et al., 2011) (Figure 2B). We also found that a fraction of ATR-interacting protein (ATRIP) was localized at the NE along with Nup153 (Figure 2C). Under unperturbed conditions, Chk1 is phosphorylated at serine 345 during mitosis, and this event is essential for viability (Wilsker et al., 2008). We found a prophase-specific NE localization of p-Chk1 that was inhibited by ATRi treatment (Figure 2D). The specificity of the anti-phospho-Ser 345-Chk1 Ab was confirmed in HU-treated cells (Figure S2). Hence, fractions of ATR, ATRIP, and p-Chk1 localize at the NE during the cell cycle, under physiological conditions; ATR association with the NE does not depend on its kinase activity. We also found that ATR and p-Chk1 distributed around the NE following aphidicoline- (Figure 2E) and hydroxyurea- (HU) (data not shown) induced replication stress. Altogether, these results are consistent with the initial hypothesis that topological stress accumulating during chromatin condensation in prophase and during chromatin replication following replication stress evokes a response at the NE that leads to ATR recruitment and activation.

Experimentally Induced Mechanical Stress Triggers the NE ATR Response Independent of DNA Damage

To more specifically address whether the NE ATR response is triggered by the NE undergoing mechanical stress, we adopted a variety of cell manipulation assays that are routinely used to induce mechanical stress at cell membranes, including osmotic stress, patch-clamp-induced cell stretching, and cell compression.

Osmotic Stress Leads to ATR Relocalization at the NE and Chk1 Activation

We first analyzed ATR distribution in response to osmotic stress, a potent inducer of mechanotransduction at cell membranes (Martins et al., 2012). Under hyperosmotic conditions, the cell and the nucleus shrink, causing NE ruffling and chromatin condensation (Martins et al., 2012). Hypotonic stress causes cell swelling and induces membrane tension but also alters the chromatin structure, apparently without causing DNA breaks (Bakkenist and Kastan, 2003).

Hypertonic and hypotonic conditions caused Chk1 phosphorylation in an ATR-dependent manner (Figure 3A). By IF,

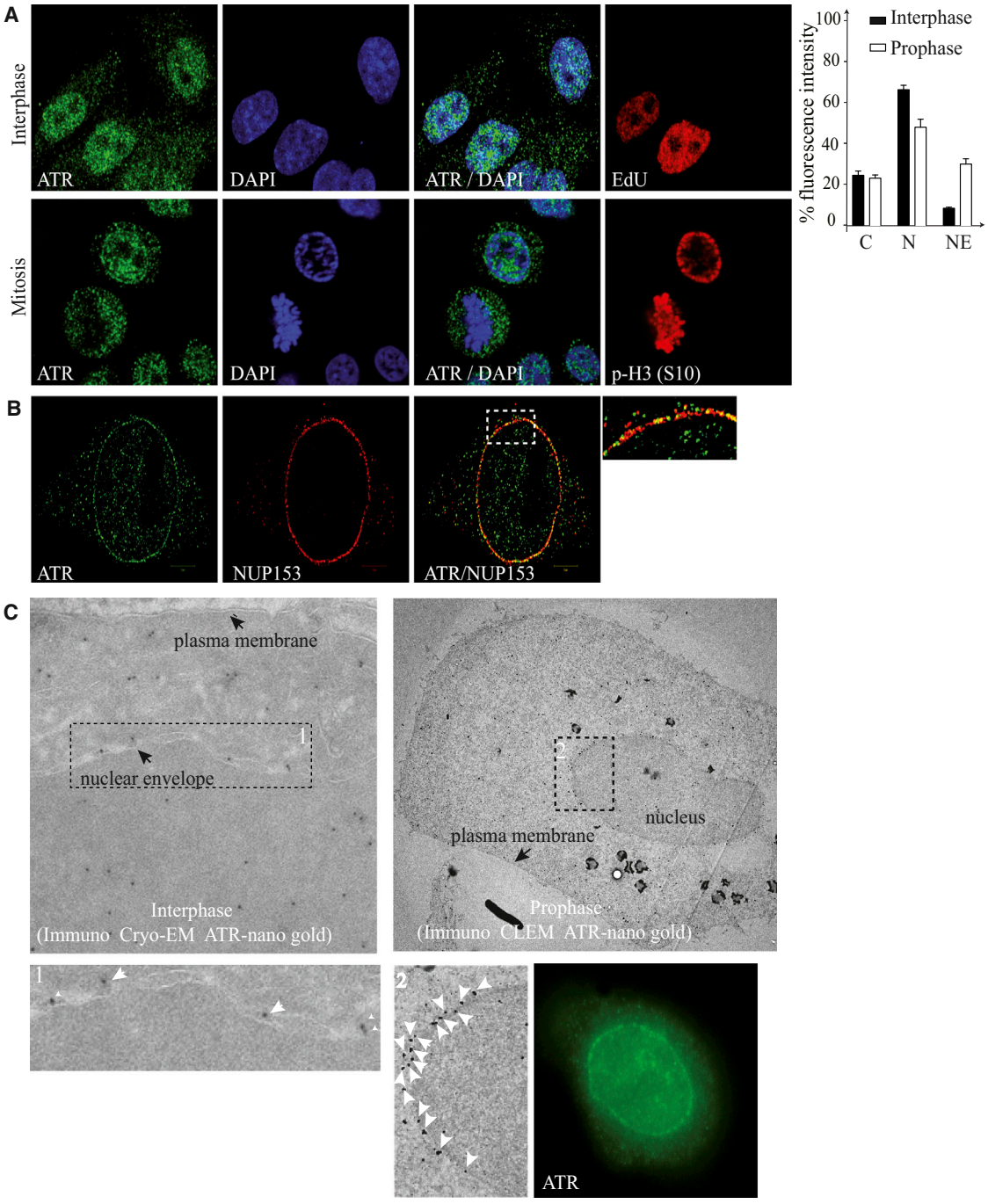

Figure 1. A Fraction of ATR Localizes at the NE during the Cell Cycle

(A) Confocal images of cells stained with anti-ATR Ab (green), DAPI (blue), EdU (red), or p-H3 (red). The graph shows the percent fluorescence intensity in the cytoplasm (C), nucleus (N), and nuclear envelope (NE) on a set of cells (n = 15).

(B) Superresolution image of a prophase cell stained with anti-ATR (green) and -NUP153 (red) Abs. A magnification is shown.

(C) Left: cryosection-based immuno-EM of an interphase cell stained with gold-tagged ATR Ab. A magnification of the selected area one (rectangle) highlights sparse ATR staining at the NE. Right: correlative light EM images of a prophase cell stained with gold-tagged ATR Ab. A magnification of the selected area two (rectangle) highlights the prominent localization of ATR at the NE. The prophase cell used to perform immuno-CLEM is shown in the lower panel, stained with anti-ATR (green) Ab.

See also Figure S1.

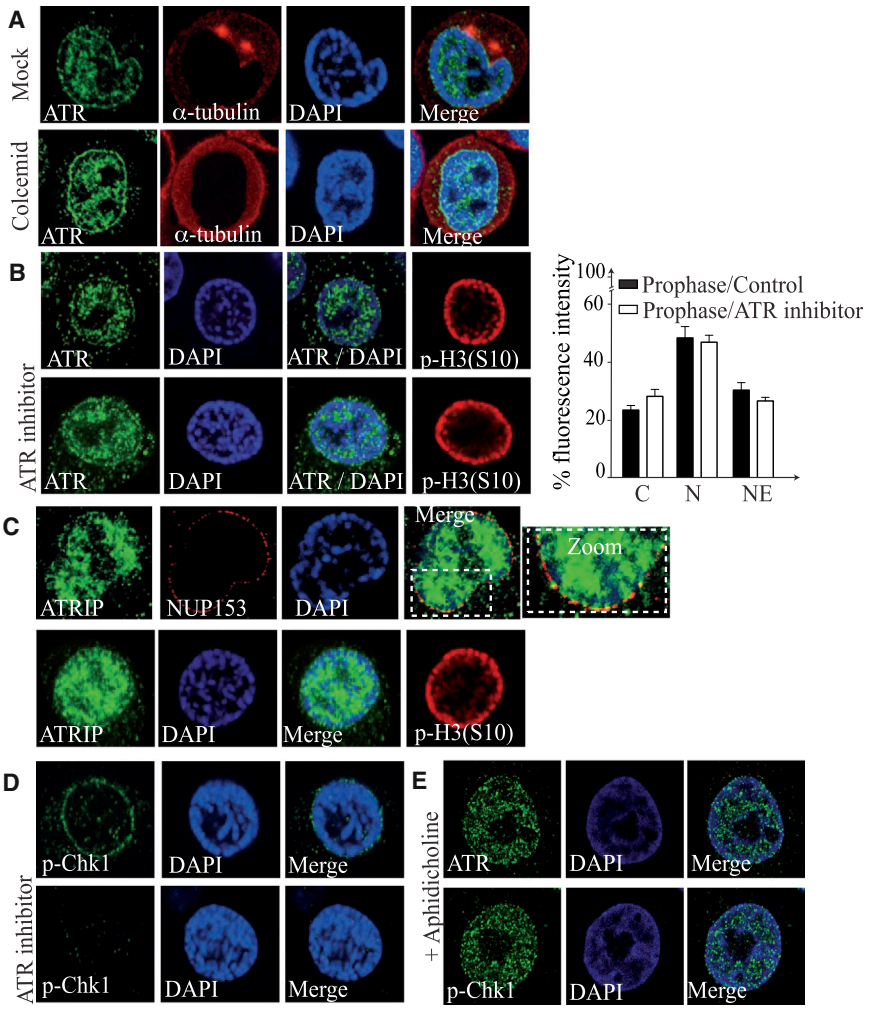

Figure 2. Checkpoint Proteins Localizing at the NE

(A) Confocal images of cells in prophase stained with anti-ATR, -α-tubulin Abs, and DAPI ± colcemid (100 nM; 2 hr).

(B) Confocal images of prophase cell stained with DAPI and anti-ATR, -p-histone H3 (S10) Abs ± ATRi (2 μM; 2 hr). The graphs show the percent fluorescence intensity on a set of cells (n = 10).

(C) Prophase cell stained with anti-ATRIP, -NUP153, -p-histone H3 (S10) Abs, and DAPI. A magnification of the dotted merged area is shown.

(D) Confocal images of NIH3T3 prophase cells stained with DAPI and anti-p-Chk1 (S345) ± ATRi (3 ± μM; 1 hr).

(E) HeLa cells were treated with aphidicholine (3 μM; 16 hr) and stained with anti-ATR, -p-Chk1 Abs, and DAPI.

See also Figure S2.

we then compared the ATR and chromatin cellular distribution in cells growing under normal conditions or treated with sorbitol (Figure 3B). Compared to untreated conditions, hyperosmotic stress caused a redistribution of ATR at the NE that did not correlate with changes in chromatin localization (Figure S3A). We observed ATR redistribution at the NE in response to sorbitol treatment in U2OS and IMR90 cells as well (Figure S3B). By time-lapse analysis in HeLa cells, we found that GFP-ATR relocalized on the NE within 30 seconds (s) following hypertonic stress (data not shown). By EM, we further investigated ATR association to the NE in cells treated with sorbitol. Whereas in isotonic conditions ATR particles accumulated mostly within the karyoplasm, in response to hypertonic stress, a significant fraction of ATR particles accumulated at the NE (Figure 3C). ATR nanogold particles localize at both the inner and the outer membranes. ATRIP and p-Chk1 also localized, in part, at the NE in response to sorbitol treatment (Figures 3D and S3C) in an ATR-dependent manner (Figure 3D). Hence, the NE is a site for ATR activation, following hyperosmotic stress. We obtained analogous results in different cell types, both cancer cell lines and normal diploid cells, and using other hyperosmotic conditions (0.4 M NaCl) (Figures S3B and S3D).

Hypotonic stress relocalized ATR at certain regions on the NE and in the nucleoli (visualized by anti-TPR Ab and by RFP-Nucleophosmin, respectively) (Figure 3E). Because mechanical signals at the cytoplasmic level can also be experienced in the nucleolus (Hu et al., 2005; Wang et al., 2009), and the nucleolus interacts with the NE (Bourgeois et al., 1979), ATR relocation at the nucleolus in response to hypotonic conditions likely reflects a response to mechanical forces, perhaps mediated by the NE and cytoskeleton (Hu et al., 2005; Maniotis et al., 1997). Given that ATR responds to DNA damage, we also determined whether hypertonic conditions induced DNA damage. We did not observe accumulation of γH2AX signals in sorbitol-treated cells, compared to untreated conditions (Figure S3D). However, γH2AX signals increased in cells treated with high NaCl doses (Figure S3D), consistent with previous findings showing that high NaCl causes DNA damage (Kültz and Chakravarty, 2001). Leptomycin-B treatment of cells exposed to hyperosmotic stress did not influence ATR localization at the NE (Figure S3E).

ATR activation by DNA damage is influenced by RPA-ssDNA nucleofilaments (Zou and Elledge, 2003). We compared ATR and RPA localization, in cells treated with or without sorbitol. RPA32 and ATR exhibited intranuclear staining (Figure 4A). Certain cells undergoing DNA replication (visualized by EdU) exhibited a perinuclear staining of RPA32 (Dimitrova et al., 1999; Vassin et al., 2009), but not of ATR. In sorbitol-treated cells, whereas ATR relocalized at the NE, RPA32 remained intranuclear. A small subset of S phase cells showed perinuclear staining of RPA32 (Figure S4A). To firmly address whether the NE translocation of ATR under hypertonic stress was RPA independent, we examined ATR and p-Chk1 localization in RPA70-depleted cells

(Figures 4B and 4C). Although RPA70 depletion affected Chk1 phosphorylation in response to HU treatment (data not shown; (Zou and Elledge, 2003), under hyperosmotic stress it neither influenced Chk1 phosphorylation (data not shown) nor influenced ATR and p-Chk1 levels at the NE (Figures 4B and 4C). Analogously, Rad17 and TopBP1, which have also been implicated in ATR activation in response to DNA damage (Duursma et al., 2013; Wang et al., 2006), were dispensable for ATR and p-Chk1 localization to the NE, in response to hyperosmotic stress (Figures S4B–S4D; data not shown). Hence, hyperosmotic stress-induced ATR relocalization and activation on the NE is RPA, Rad17, Tobp1, and DNA damage independent.

Whole-Cell Mechanostimulation Targets ATR to the NE

We then used an alternative method to induce mechanical stimulation at cell membranes. In this case, a patch-clamp-automatized platform was employed to stretch the cell using two glass pipettes placed on the plasma membrane at opposite poles in cell-attached configuration (Figure 5A). We reasoned that plasma membrane stretching propagates the mechanical stimulation to the NE promoting structural rearrangements within the nucleus (Wang et al., 2009). By moving the pipettes apart, we induced in HeLa cells a mechanical stretch of the plasma membrane and followed the distribution of GFP-ATR (Figure 5A; Movie S1). ATR rapidly redistributed at perinuclear regions overlapping with the lamin A signal. ATR perinuclear localization initiated at the focal points of the mechanical tension and progressively distributed along adjacent NE areas. We observed an accumulation of GFP-ATR in the nucleolus as well (Figure 5A). We addressed whether the pipette-mediated cell deformation caused chromatin condensation as in the case of nuclear deformation (Shivashankar, 2011) (Figure 5B). We will refer to this phenomenon as force-induced chromatin compaction, to distinguish it from the chromatin condensation process taking place in prophase. Concomitantly with the accumulation of GFP-ATR in the nucleolus, 30 s after pipette mechanostimulation, chromatin compaction was evident, as shown by the m-cherry H2B distribution. Subsequently, GFP-ATR localizes at the nuclear periphery. We consistently observed that mechano-induced GFP-ATR redistribution at the nucleolus and/or at the NE paralleled chromatin compaction and that the association of ATR to the nucleolus anticipated the ATR localization at the NE (data not shown). Again, by comparing the distribution of ATR and chromatin following cell stretching, we observed no spatial correlation between chromatin movement and ATR relocalization (Figure 5B). Mechanical forces can be transferred by transmembrane receptors that convert mechanical stimuli into biochemical signals to modulate various intracellular functions (Mammoto et al., 2012). In particular, calcium ions are the most rapid mediators of mechanical stimuli. However, in the case of ATR, extra/intracellular calcium chelation using BAPTA did not affect GFP-ATR cellular redistribution following mechanical stress (data not shown). Mechanostimulation by pipettes did not cause accumulation of DNA damage as assessed by examining γ-H2AX foci (Figure S5A).

The procedure described above has some limitations because it is based on glass pipette-attached cell stretching and does not allow us to study the recovery from the mechanostimulation. Therefore, to determine whether the mechanical forces inducing ATR redistribution are within the physiological range of forces experienced by cells in soft tissues and whether the ATR mechanical response is reversible, we used the compressive-load system (CLS) (to exert forces in the approximate range of 1 to 1,000 nN (Figure 5C). Using CLS, which is based on weights that impose deformations on cells by axial compression, it is possible to approximately estimate the magnitude of the forces applied to induce the ATR response and to study the recovery from compression, after unloading the weights. When we applied CLS on HeLa cells cotransfected with GFP-ATR and m-cherry H2B (Figure 5C), GFP-ATR redistributed at perinuclear regions and in the nucleolus. The ATR localization in the nucleolus anticipated the perinuclear redistribution of ATR. Approximately 15–30 nN forces were needed to visualize ATR relocation. When we unloaded the weights, both the nucleolus and the nuclear envelope rapidly lost the GFP-ATR signal, and ATR assumed the typical distribution of unstressed cells (Figure S5B). Recovery of ATR distribution paralleled chromatin decompaction (Figure S5B). Hence, ATR responds to mechanical stimulation of the plasma membrane and to cell compression. Following mechanical stress, the ATR redistribution to the nucleolus precedes the ATR localization to the nuclear envelope. This perhaps reflects a differential viscoelastic response of these two cellular compartments. The ATR response to mechanical stress occurs at physiological range of forces and is fully reversible. Moreover, the changes in ATR cellular distribution, following activation and recovery upon mechanical stress, parallels chromatin compaction and decompaction, respectively.

ATR Influences the Coordination between Chromatin Condensation and NEBD

The above data show that mechanical stress induces an ATR NE response, suggesting a role for ATR in coordinating chromatin dynamics and NE metabolism in response to mechanical stimulations. To address this intriguing concept in a physiological scenario, we next monitored the kinetics of chromatin condensation and NEBD in HeLa cells, cotransfected with GFP-H2B and RFP-Lamin A, prearrested in G2 with a CDK1 inhibitor, and released into mitosis with or without active ATR (Figure 6A). In cells released into mitosis with a functional ATR, chromatin condensation began at 20 min, was nearly completed by 30 min, and reached the typical metaphase configuration at 70 min. At 20 min a fraction of lamin A was still tethered to the partially condensed chromatin. By 30 min, NEBD was completed and lamin A was totally dissolved. In cells entering mitosis with pharmacologically inactived ATR, the onset and the completion of chromatin condensation were significantly delayed: it started at 75 min and completed around 115 min. A fraction of lamin A was still visible and attached to the condensed chromatin until 85 min. NEBD and lamin A disintegration were observed, but after 115 min. To rule out that the uncoordinated chromatin condensation and NEBD observed in ATR-inhibited cells was due to DNA damage left unresolved because of the absence of ATR activity, we analyzed γ-H2AX foci by IF (Figure S6). We observed comparable γ-H2AX foci numbers in control and ATR-inhibited cells in mitosis. To further confirm the above observations, we used human primary fibroblasts from Seckel patients, who carry hypomorphic mutations in the *ATR* gene

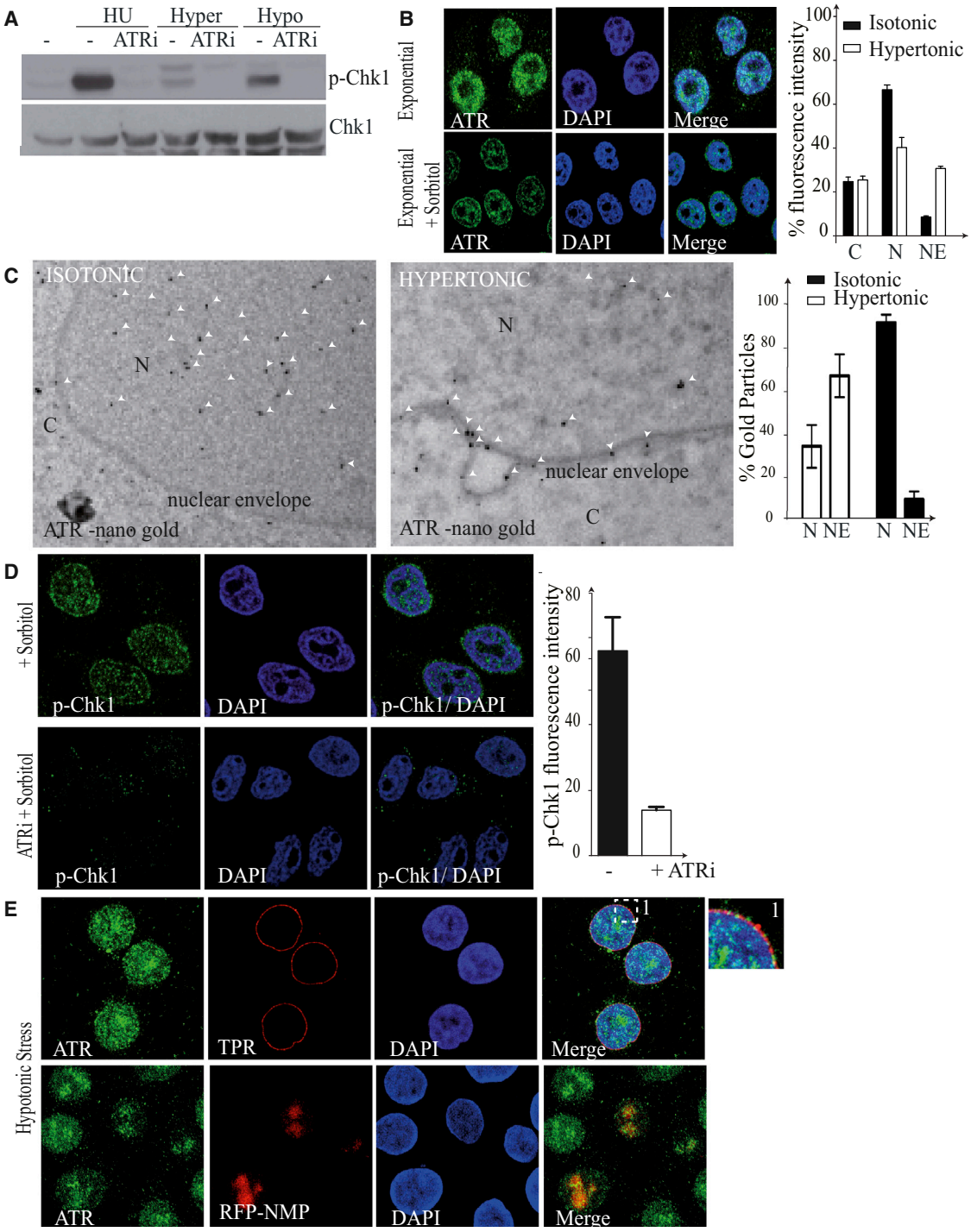

Figure 3. Osmotic Stress Induces ATR Relocalization at the NE

(A) HeLa cells were incubated with DMSO or ATRi (3 μM; 2 hr) and treated with HU (10 mM; 1 hr) and then hypertonic media (40 min) or hypotonic media (40 min), respectively. Cells were examined by western blot using anti-p-Chk1 and Chk1 Abs.

(B) HeLa cells were exposed to mock or hypertonic medium (0.5 M sorbitol; 20 min) and stained with anti-ATR Ab (green) and DAPI (blue). The graphs show the percent fluorescence intensity on a set of cells (n = 50).

(C) Immuno-cryo-EM images of HeLa cells stained with gold-tagged anti-ATR Ab under normal or hypertonic conditions. White arrows highlight ATR gold particles. The graph represents the percentage of ATR-related nanogold particles in isotonic or hypertonic conditions in the nucleoplasm or at the nuclear envelope.

(legend continued on next page)

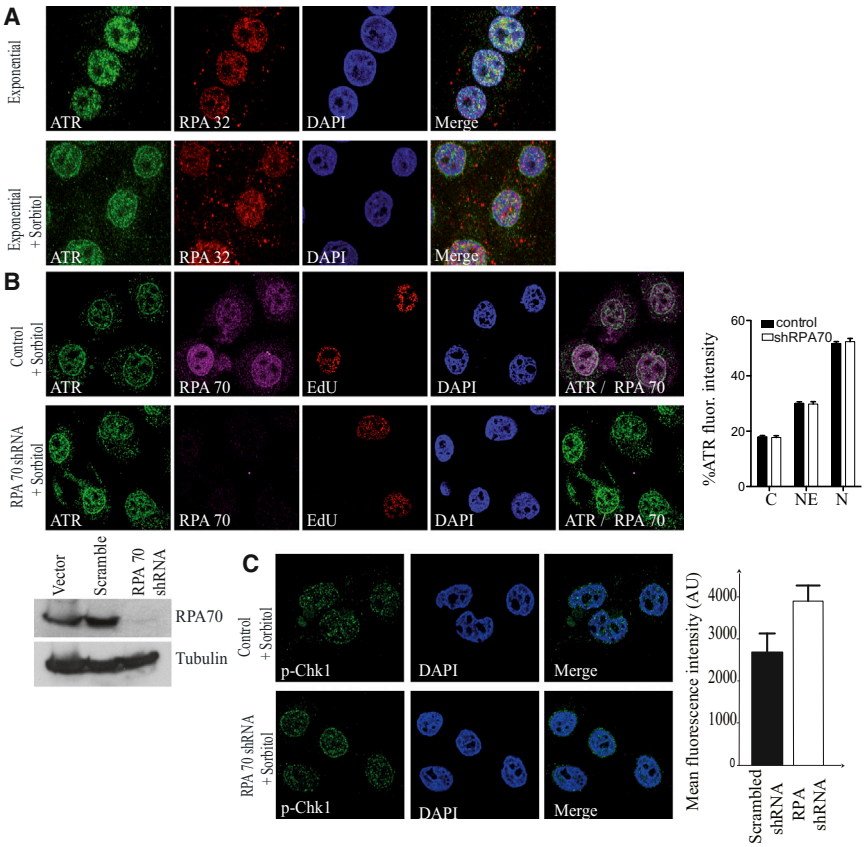

Figure 4. ATR Activation at the NE Does Not Depend on RPA

(A) Confocal images of HeLa cells exposed to normal or hypertonic medium (0.5 M sorbitol; 20 min). Samples were stained with anti-ATR (green), -RPA32 (red) Abs, and DAPI.

(B) HeLa cells were transfected with empty vector or RPA70 shRNA and selected with 3 μg/ml puromycin (72 hr). Cells were incubated with hypertonic medium containing 0.5 M sorbitol for 20 min and stained with anti-ATR (green), -RPA70 (magenta) Abs, S-phase-specific EdU (red), and DAPI (blue). RPA70 protein levels were analyzed by western blot using anti-RPA70 Ab and anti-tubulin as a loading control (lower panel). The graph shows the percent ATR fluorescence intensity in different cellular compartments on a set of cells (n = 20).

(C) Puromycin-selected RPA70 shRNA-transfected HeLa cells were incubated with hypertonic medium containing 0.5 M sorbitol for 30 min and stained with p-Chk1 (green) and DAPI (blue). Graphs show the integrated p-Chk1 fluorescence intensity on a set of cells (n = 20). Quantitative analysis of P-Chk1 levels is shown.

See also Figure S4.

(O'Driscoll et al., 2003) (Figure 6B). As above, control and Seckel cells were prearrested with a CDK1 inhibitor and released into mitosis. In control cells, chromatin condensation and NEBD were evident already at 15 min and completed by 30 min; metaphase cells were observed at 75 min. In contrast, in Seckel cells, chromatin condensation and NEBD were delayed; at 30 min, intact NEs were still observed; at 45 min, cells exhibiting condensed chromatin attached to large portions of lamin A were detected; and complete NEBD and chromatin condensation were visualized only at 75 min. Analogously, when we used mouse embryonic fibroblasts derived from humanized ATR hypomorphic Seckel mice (Murga et al., 2009), under the same experimental conditions, we observed a 30 min delay in chromatin condensation and NEBD (data not shown).

Thus, in ATR-defective cells, the initiation and completion of chromatin condensation and NEBD are delayed; moreover, portions of lamin A remain associated with condensed chromatin even after the NEBD, suggesting a defect in detaching condensed chromatin from the NE. Similar defects were also observed in Seckel cells (Alderton et al., 2004).

DISCUSSION

In this study, we showed that in human and mouse cells grown under unperturbed conditions, a fraction of ATR, ATRIP, and pChk1, key components of the ATR signaling cascade, accumulate at the NE. Our working model is that ATR responds to chromatin dynamics in S phase (particularly under replication stress) and prophase, when chromatin replication and condensation generate topological stress that is converted into mechanical stimuli. Whereas our previous findings in yeast indicated replication stress as a major cause of mechanical stress on the nuclear membrane (Bermejo et al., 2011), our current data in mammalian cells may suggest that ATR plays a more prominent role at the NE in prophase when chromatin condensation occurs. This might reflect the magnitude of forces acting during chromatin condensation/decondensation (Mazumder et al., 2008), which is greater than the forces acting during DNA synthesis and/or important differences between chromatin condensation and chromatin replication from the topological point of view. During prophase chromatin condensation causes torsional stress, whereas during an unperturbed S phase, moving replication forks are assisted by DNA topoisomerases that travel with the forks (Bermejo et al., 2007) and prevent the accumulation of torsional stress. However, given our previous results during S phase in yeast, it is possible that transient mechanical

(D) HeLa cells were incubated with DMSO or ATRi (ATRi), followed by treatment with hypertonic medium (0.5 M sorbitol; 20–30 min) and stained with anti-p-Chk1 Ab (green) or DAPI (blue). The graphs show the mean fluorescence intensity on a set of cells (n = 10).

(E) Top: HeLa cells were incubated in hypotonic medium and stained with anti-ATR Ab (green), anti-TPR Ab (red), and DAPI (blue). A magnification of the merged ATR, TPR, and DAPI is shown. Bottom: RFP-NPM-transfected cells were treated as in the top panel and stained with anti-ATR Ab and DAPI.

See also Figure S3.

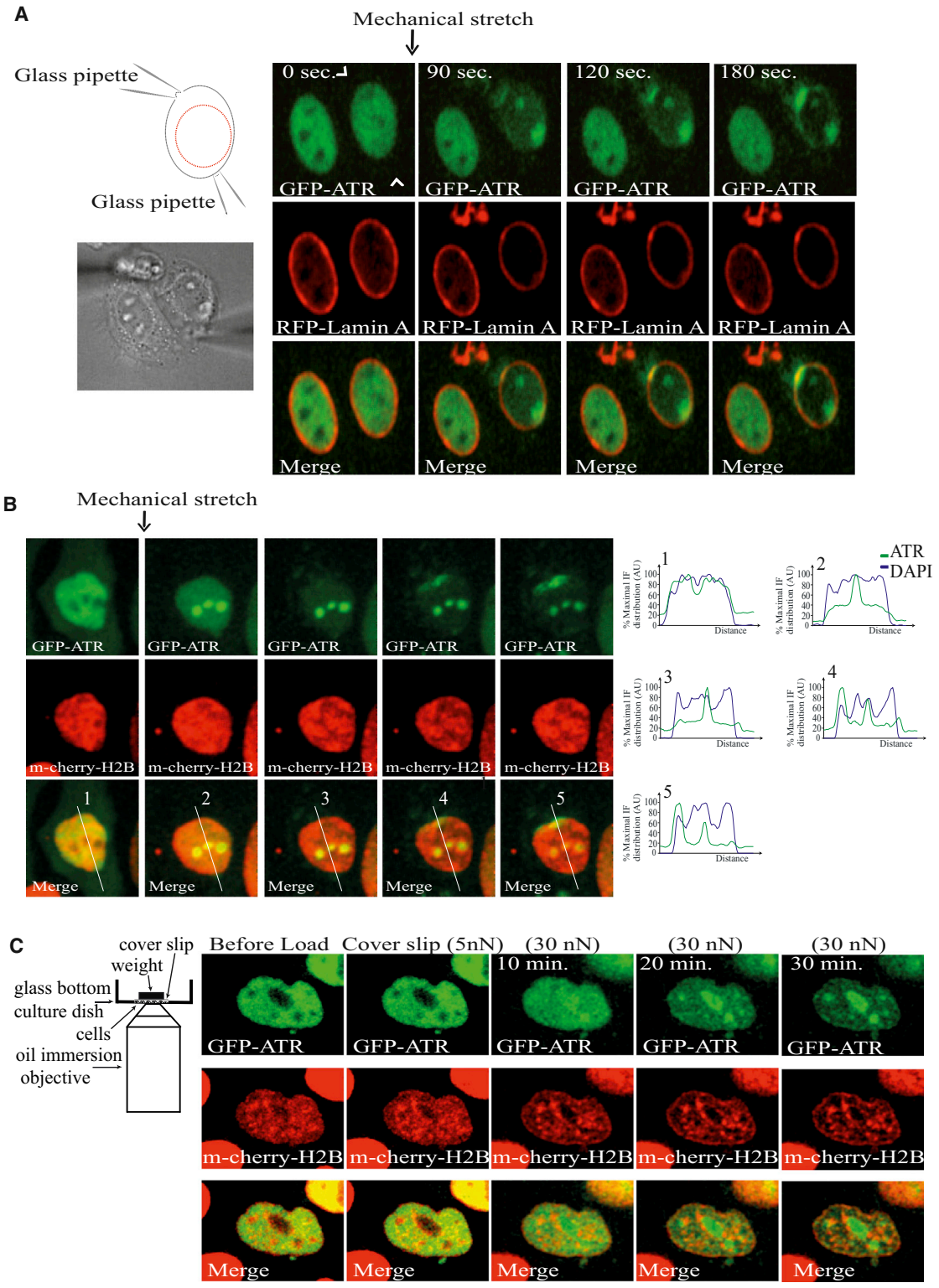

Figure 5. ATR Responds to Mechanical Forces Acting on Membranes

(A) Schematic representation of two-patch-clamp pipettes positioned on the two opposite sides of the plasma membrane. The corresponding microscope image is on the left. The white arrows indicate the points of focal tension induced by the mechanical stretching. Two patch pipettes were attached to the plasma membrane of a HeLa cell coexpressing GFP-ATR (green) and RFP-Lamin A (red) and stretched to induce mechanical stress on the membranes. The intracellular changes in GFP-ATR localization was examined in real time with a gap of 30 s.

(legend continued on next page)

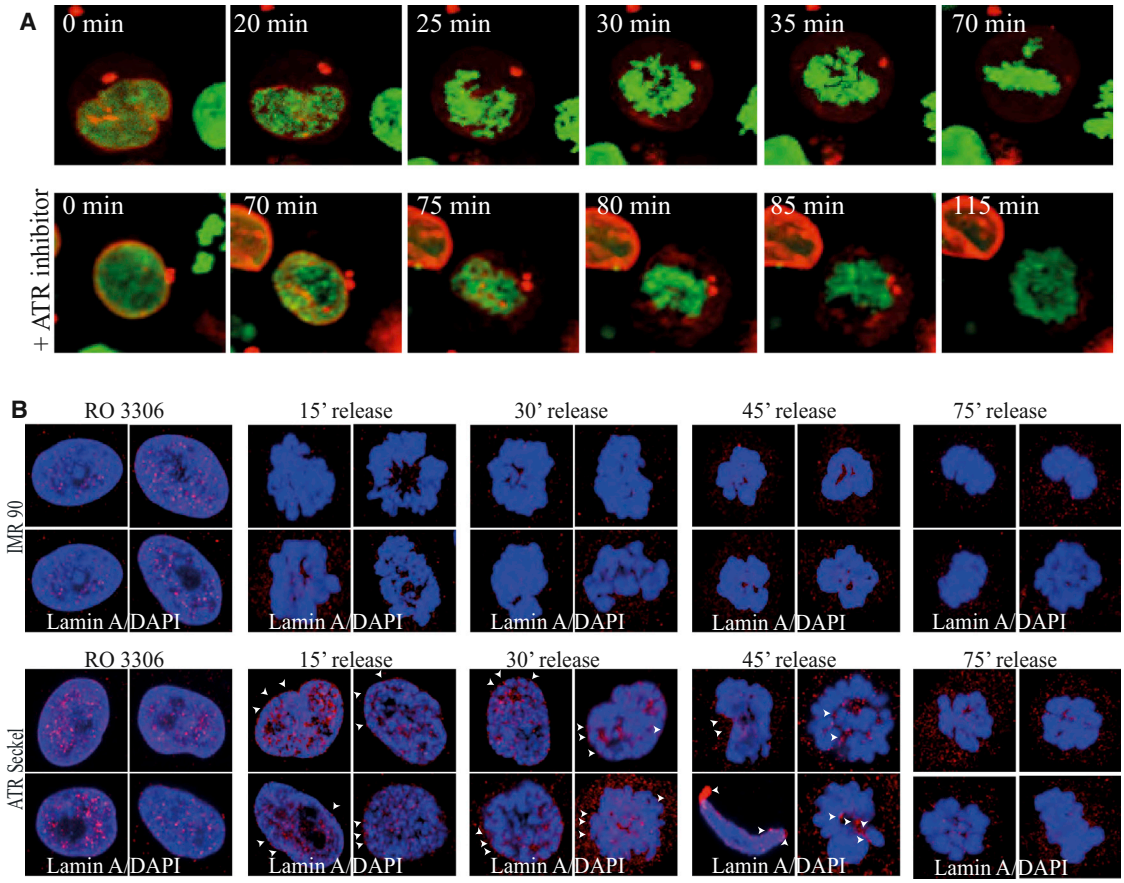

Figure 6. ATR Coordinates Chromatin Condensation and NEBD

(A) RFP-Lamin-A-transfected GFP-H2B HeLa cells were arrested in G2 with the R3306 Cdk1 inhibitor (10 μM, 16 hr), followed by incubation with DMSO or ATRi (3 μM, 1 hr). Later, the cells were released into mitosis ± ATRi, and cells entry into prophase and metaphase was examined. A representative image of n = 10 is shown.

(B) Same as in (A), IMR90 and *ATR*$^{s/s}$ human fibroblasts were arrested in G2 with Cdk1 inhibitor R3306 (10 μM, 16 hr), followed by release in mitosis. Cells were fixed and stained for anti-Lamin A (red) and DAPI (blue) at represented time intervals postrelease.

See also Figure S6.

signals are generated when forks approach LADs. Although we did not observe association of ATR to the NE during unperturbed S phase in mammalian cells, there might be a transient relocalization spread over the several hours that normal S phase lasts. Perturbing S phase with, aphidicolin- or HU-induced replication stress, which would stall replication forks and generate a persistent mechanical signal at the NE, did indeed trigger accumulation of ATR at the NE.

Further work will be required to determine how mechanosensing influencing ATR localization occurs. NE portions connecting two adjacent LADs may act as mechanosensors of local chromosomal forces and undergo changes in membrane fluidity and/or curvature. Changes in membrane fluidity might muffle mechanical stress and eventually transduce the signal to ATR. This is consistent with the observations that membrane fluidity is modulated in response to a variety of stress conditions (Aguilar and de Mendoza, 2006; Vigh et al., 2007), including HU treatment (Fujikawa-Yamamoto and Odashima, 1989). The relative abundance of polyunsaturated fatty acids influences nuclear membrane fluidity and ATR activation (Zhang et al., 2007b).

(B) Same as in (A), two patch pipettes were attached to the plasma membrane of a HeLa cell coexpressing GFP-ATR (green) and m-cherry H2B (red) and stretched to induce mechanical stress on the membranes. The intracellular changes in GFP-ATR and chromatin-associated H2B localization were examined in real time. The graphs illustrate the quantification in arbitrary units (a.u.) of the distribution of GFP-ATR and m-cherry-H2B by IF along the lines shown in the merged panels.

(C) Schematic representation of the setup used to perform compressive load experiments (left panel). GFP-ATR and m-cherry-H2B-transfected cells were compressed with 30 nN forces using weights, and the intracellular changes in GFP-ATR localization and chromatin architecture (m-cherry H2B) were examined in real time with a gap of 10 min. A representative image of n = 10 is shown.

See also Figure S5 and Movie S1.

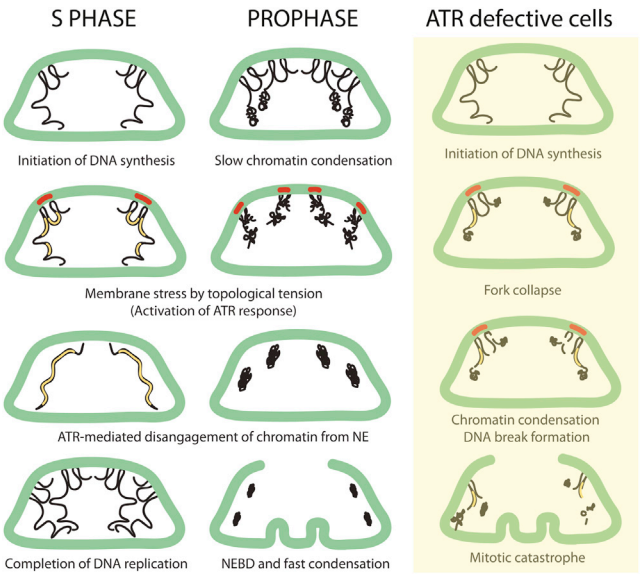

Figure 7. A Model Describing ATR-Mediated Events in S Phase and Prophase at the Nuclear Envelope

The model integrates the observations deriving from yeast studies (Bermejo et al., 2011) focused on the S phase function of the ATR pathway, with the findings described in this paper. The nuclear envelope is shown in green; the chromosomes are shown in black; and the replicons are shown in yellow. The red bars at the envelope indicate the nuclear membrane areas exposed to mechanical stress. Briefly, nuclear envelope-associated chromatin transfers the mechanical forces arising from the topological transitions of replicating or condensing chromosomes to the nuclear envelope. Local nuclear membrane stress recruits ATR. The ATR response then coordinates chromosome replication and condensation with the nuclear envelope by modulating chromatin and nuclear envelope association. In ATR-defective cells, the inability to coordinate replication with the nuclear envelope at those chromatin regions associated to the lamin, causes fork collapse. The partially replicated chromatin remains in part associated to the NE when condensation begins, thus leading to progressive chromatin fragmentation and mitotic catastrophe.

Membrane fluidity can influence its curvature (McMahon and Gallop, 2005). Notably, we observed that ATR is enriched at NE invaginations, structures that are known to arise in response to mechanical forces (Beaudouin et al., 2002).

ATR recruitment to the NE in response to membrane stress does not require its kinase activity. We speculate that, in response to mechanical stimuli, ATR is part of a multistep activation process involving (1) changes in nuclear membrane fluidity and/or curvature, (2) ATRIP and ATR recruitment at the NE, and (3) ATR kinase activation in an unorthodox manner independent of RPA and DNA damage. The observation that the N terminus of ATR exhibits elastic properties (Grinthal et al., 2010; Perry and Kleckner, 2003), whereas the kinase domain represents a small portion of the C terminus, makes ATR an ideal module to respond to mechanical stimuli, perhaps through a mechanism mediated by its elastic domain. Interestingly, TORC2 has been implicated in the cellular response to membrane stress (Berchtold et al., 2012) and shares homology with ATR (Perry and Kleckner, 2003).

Based on our present data in mammalian cells and on previous findings implicating the yeast ATR ortholog Mec1 in detaching chromatin from the NE in S phase (Bermejo et al., 2011), we propose that, during unperturbed cell cycles, the recruitment of ATRIP-ATR at the NE contributes to coordinate chromatin and NE dynamics, in S phase, as well as in prophase (Figure 7). Chromosome replication and condensation, besides being topologically complex, are influenced by the NE. However, there are key evolutionary differences between *Saccharomyces cerevisiae* and higher eukaryotes that may explain certain species-specific aspects of the ATR pathway. In yeast, the NE does not breakdown and chromatin condensation never reaches the level of complexity seen in mammalian cells. In fact, the yeast Mec1/ATR pathway is prominently involved in the coordination of S phase events through Rad53, whereas Chk1 plays a minor role. However, certain *mec1* alleles exhibit the typical features of ATR-deficient cells (Cha and Kleckner, 2002). In human cells, chromatin condensation begins slowly at 30 min before NEBD and proceeds more rapidly following the envelope breakdown (Beaudouin et al., 2002). Thus, in mammals, the coordination between chromatin condensation and NE breakdown likely plays a key role in preventing aberrant chromosomal dynamics. Accordingly, Chk1 plays a pivotal function in human cells, and inactivation of ATR causes aberrant chromatin condensation and NEBD (Nghiem et al., 2001). Hence, whereas in mammals ATR might be mainly involved in coordinating the topological complexity of chromatin condensation with NE dynamics (while still performing important functions in S phase, particularly under enhanced replication stress), in yeast it might be primarily required to deal with the topological problems arising at perinuclear chromatin in S phase (Bermejo et al., 2011). The fact that chromatin condensation starts at a low rate, while the NE is still intact, may reflect the topological complexity of condensing the chromatin fiber, where there are still chromatin regions bound to the envelope and that may be the reason why, following NEBD, condensation is faster. We propose that ATR responds to the topological tension when condensation begins, binds the NE, and facilitates the condensation process by progressively resolving the LADs. This is consistent with our finding that ATR-inhibited/mutated cells are delayed in the processes, leading to chromatin condensation and NEBD (Figure 6) and with the observation that Seckel cells exhibit nuclear fragmentation, while the chromatin is still attached to the NE (Alderton et al., 2004). Moreover, ATR has been implicated in the phosphorylation of condensin subunits, as well as of NE proteins (Matsuoka et al., 2007). According to the scenario we propose, the inability to regulate the association between the chromatin and the NE in response to mechanical stimuli arising from topological transitions might have the following consequences: in S phase cells, the chromatin fiber would remain in part attached to the envelope, thus causing fork collapse. Attempts to condensate a partially replicated chromatin, still bound to the NE, would generate DNA breaks and aberrant condensation events (Figure 7). Indeed, ATR-deficient cells exhibit some of these defects (Brown and Baltimore, 2003; Cha and Kleckner, 2002; Nghiem et al., 2001). Intriguingly, recent observations showed that fragile site expression in *mec1* mutants is mediated by condensins and DNA topoisomerase II (Hashash et al., 2012). The nuclear fragmentation phenotype of Seckel cells (Alderton et al., 2004; O'Driscoll et al., 2003) can be expressed only if cells have

previously undergone fork collapse and occurs when the NE is still intact. In our experimental conditions (Figure 6), we did not observe nuclear fragmentation as cells passaged through the preceding S phase with a functional ATR.

One intriguing aspect of our present data set is the result that the classical DNA damage-induced ATR activation pathway, which is influenced by RPA, TopBP1, and the 9-1-1 complex, is genetically uncoupled from the ATR response to mechanical stress. Given the large number of nuclear and nonnuclear targets modulated by ATR, it is reasonable to think that ATR might be engaged in at least partly different pathways in response to different stimuli. One possibility is that the RPA-ssDNA-mediated signaling generates the context for engaging ATR when cells experience genotoxic insults, whereas the membrane-dependent checkpoint activation may be more confined to a physiological context to sense subtle chromatin dynamics. However, certain insults, such as replication stress, might trigger both ATR responses, by accumulating single stranded DNA at forks (Toledo et al., 2013) and topological stress at perinuclear chromatin (Bermejo et al., 2011).

Given that partially condensed silenced chromatin has a tendency to localize at the nuclear periphery (Shevelyov and Nurminsky, 2012), an ATR response regulating chromatin-lamin association in response to membrane stress might have important epigenetic implications.

During S phase and prophase, the ATR relocation at the NE likely reflects a physiological response triggered by the topological stress arising from chromatin dynamics and transmitted to the NE through LADs. Conversely, osmotic stress and mechanical stimuli may lead to more dramatic cell deformation, membrane stress, and chromatin rearrangements. Under osmotic stress conditions, the response is likely triggered by membrane stress directly. The pipette-induced mechanical stimulation of the plasma membrane might be instead transduced to the NE by the cytoskeleton (Wang et al., 2009). Finally, CLS-induced cell deformation mimics the context of interstitial migration in which the nucleus has to squeeze through pores. CLS and interstitial migration cause mechanical stress at the NE and chromatin condensation (Friedl et al., 2011; Gerlitz and Bustin, 2010; Wolf and Friedl, 2009).

Altogether, our observations suggest that ATR is needed to protect the perinuclear chromatin from mechanical insults induced by a variety of mechanical stimuli. This might be achieved by controlling the association of chromatin to the lamin but also by controlling cytoskeleton organization as also suggested by recent observations (Enserink et al., 2006; Kremer et al., 2007). The ATR pathway may therefore rapidly connect external signals with epigenetic modifications in the nucleus, thereby contributing to coordination of membrane signaling with gene expression, and protecting the chromatin and genome integrity.

EXPERIMENTAL PROCEDURES

Reagents and cDNAs

ATR, p-CHK1 (S345), RPA70, and p-histone H3 (Ser10) antibodies were obtained from Cell Signaling; ATRIP, NUP153, and RPA32 were obtained from Abcam; TPR, γH2AX (S139), and lamin A Abs were obtained from Sigma and Millipore; and Chk1 was obtained from Leica. EdU (click-IT), RPA70-, TopBP1-, and RAD17-small hairpin RNAs (shRNAs) were obtained from Invitrogen and Origene Technologies, respectively. ATR-specific inhibitor and ATR shRNA were from Dr. Oscar Capetillo (Centro Nacional de Oncologia [CNIO]) (Toledo et al., 2011); the GFP-ATR plasmid was from Dr. Randal Tibbetts (Tibbetts et al., 2000); RFP-Lamin was from Prof. Howard J. Worman (Columbia University) (Ostlund et al., 2006); and RFP-Nucleophosmin was a gift by Dr. Michelle Hill (University of Queensland). GFP-H2B and m-cherry-H2B were from IFOM. Colchicine, α-tubulin Ab, Leptomycin B, Hydroxy Urea, sorbitol, Aphidicholine, and R3306 CDK1-specific inhibitor were obtained from Sigma.

Cell Culture, Transfection, Treatments, and Cell Lysis

HeLa, U2OS, NIH 3T3, and mouse embryonic fibroblasts cells were maintained in complete medium as described (Kumar et al., 2006). Media were supplemented with 0.5 M sorbitol (or 0.4 M NaCl) for hypertonic conditions or diluted 1:5 with MQ water for hypotonic conditions. IMR90 and Human Seckel cells (Coriell Cell Repository) were grown in Eagle's minimum essential medium (MEM; GIBCO-BRL), supplemented with nonessential amino acids, 10% (vol/vol) fetal bovine serum (not activated), 2 mM glutamine, 10 mM HEPES, 100 U/ml penicillin, and 100 μg/ml streptomycin in a humidified atmosphere (5% CO2, 37°C). We used lipofectamine 2000 (Invitrogen) for transfection. Cells transfected with ATR shRNA or RPA70 shRNA were selected for 72 hr in medium plus 3 μg/ml puromycin. For hyperosmotic stress experiments, exponentially growing cells were seeded on dishes and after 24 hr, the medium was replaced with hypertonic medium and incubated for 20–30 min for ATR and for 30–40 min for p-Chk1 experiments, before harvesting or fixing the cells. For hypotonic stress conditions, cells were exposed to hypertonic medium for 2–5 min before fixation. Total cell lysates were prepared in RIPA lysis buffer (Marqués et al., 2009). To arrest cells in G2 phase, GFP-H2B and RFP-Lamin-A-transfected HeLa cells were treated with 10 μM R3306 for 16 hr and were later washed three times with complete medium followed by release in mitosis ± ATR inhibitor.

Immunofluorescence

For IF assays, cells were processed as previously described (Kumar et al., 2010, 2011). In brief, cells were fixed with 4% formaldehyde (10 min), blocked, and permeabilized with 0.3% TX-100 PBS (20 min) and incubated with primary antibodies (ATR and p-Chk1 1:50, TPR, p-histone H3 and NUP153 1:500, p-H2AX, RPA32, ATRIP, and RPA70 1:200, and lamin A/C 1:200) in blocking buffer (1 hr, room temperature [RT]), followed by three washes. Species-specific secondary antibodies were added to samples and incubated (1 hr, RT), followed by three washes with blocking buffer. Samples were mounted on coverslips with mounting medium containing DAPI (VectaShield); cells were then visualized and captured using Leica TCS SP2 confocal scanning microscope, equipped with a 63×/1.4 NA objective. Single optical sections of the images were used to represent the staining with different antibodies, and images were processed using ImageJ and smoothed to reduce the background noise. For SR-SIM superresolution microscopy, cells were grown on glass coverslips and fixed with 4% formaldehyde (10 min.). IF staining was performed as described above, with primary antibodies (NUP153 1:500, ATR 1:50) incubated for 16 hr at 4°C. Samples were mounted by mounting medium with DAPI (VectaShiled) and covered by coverslips. Images were acquired using Zeiss Axioimager Z.1 platform equipped with the Elyra PS.1 superresolution system for SR SIM using Zeiss objectives Alpha Plan Apochromat 63×/1.40 NA oil objective (total magnification 1,008×) and Plan Apochromat 100×/1.46 NA oil objective (total magnification 1,600×) with appropriate oil (Immersol 518F). Images were captured with an EM-CCD camera (Andor iXON EM+; 1004 × 1002 px, cooled at −64°C, 16-bit) at typical exposure times varying between 80–200 ms and with gain values between 20–25. SR-SIM setup included five rotations and five phases of the grated pattern for each image layer. The z stacks were acquired in 110 nm sections for 63×/1.40 NA, 101 nm for 100×/1.46 NA objectives. All acquisitions, SIM calculations and measurements of colocalization were performed in the Zeiss Zen software (v. 11) (Zen Blue version, Carl Zeiss Microscopy).

Fluorescence Intensity Quantification

We used ImageJ to quantify the integrated fluorescence intensity (FI) of the 8-bit images. A cell was divided in three compartments: nucleus, nuclear envelope (including inner and outer nuclear membranes), and cytoplasm. The nuclear area was defined using NUP153 as nucleus boundary. The NUP153-stained region was considered the nuclear envelope. We calculated the integrated intensity of the whole cell, the nucleus (N), and nucleus including out nuclear envelope (NIO). The nuclear envelope-associated fluorescence was determined by subtracting the FI in nucleus from FI in NIO. To measure the cytoplasm-linked FI, NIO-associated FI was subtracted from the whole-cell FI. The percent FI in each compartment was calculated as a fraction of whole-cell FI. To compare the movement (redistribution) of ATR and chromatin, following isotonic/hypertonic stress or cell stretching, a line was drawn across the cell in a region of interest (where significant ATR localization was evident) and the relative fluorescence signals (ATR and DAPI or GFP-ATR and m-cherry H2B) were measured along the lines using plot profile (ImageJ). The graphs were plotted as the percent of maximal intensity of the corresponding fluorescence signals along the region of interest.

Electrophysiology

The two-electrode patch-clamp technique has been used to mechanically and electrically manipulate the cell. Glass patch pipettes were prepared using a Flaming/Brown P-97 micropipette puller (Sutter Instrument) and fire polished to a tip diameter of 1–2 mM in diameter. The electrodes were filled with a solution containing (in mM) 140 KCl, 10 NaCl, 2.5 $CaCl_2$, 1 $MgCl_2$, 10 HEPES, 10 Glucose (pH 7.4). Current and voltage were monitored using a 700B Axon amplifier (Molecular Device) and elaborated with PClamp 10 software (Molecular Device). Cells were approached using two motorized micromanipulators (Luigs and Neumann) mounted on the microscope stage. Immediately after induction of mechanical stretch, repeated images (we acquired z stacks time-lapses in most cases, and not single plane time-lapses) of the same field were acquired on a UltraVIEW VoX spinning-disc confocal unit (PerkinElmer), equipped with an Eclipse Ti inverted microscope (Nikon) and a C9100-50 electron-multiplying CCD (charge-coupled device) camera (Hamamatsu). We used a Nikon objective Plan Fluor 40×/1.30 NA. All components were controlled by Volocity software (PerkinElmer). Time-lapses were recorded with a time frame of 30 s per z stack for double patch experiments. The images were processed using ImageJ and smoothed to reduce the background noise.

Electron Microscope Imaging

Routine electron microscopic examination and immuno-EM labeling based on pre-embeding, cryosectioning, and correlative light-electron microscopy were performed as previously described (Kweon et al., 2004; Mironov and Beznoussenko, 2009, 2012; Polishchuk et al., 1999). Cells (5–8) were counted for estimating the number of ATR-tagged gold particles in different compartments of the nuclei including nuclear envelope. Percentage of labeling on the nuclear envelope and nucleoplasm was estimated in the following way: gold particles localized within 20 nm from the nuclear envelope were considered as being on the nuclear envelope. All other particles were considered as localized within the nucleoplasm.

Compressive Load System

To apply quantitative forces on cells, different weights (2–4 g) were put on the coverslip mounted on the cells. The approximate magnitude of force/cell was calculated considering the total area of the coverslip, number of cells seeded, and the weight applied on the coverslip.

$$\text{Force/cell} = \text{Pressure under coverslip} \times \text{Total area of cells N/Total number of cells under coverslip}$$

$$\text{Pressure} = \text{Weight applied} \times 9.8\ \text{N/m}^2/\text{Area of coverslip}$$

SUPPLEMENTAL INFORMATION

Supplemental Information includes six figures and one movie and can be found with this article online at http://dx.doi.org/10.1016/j.cell.2014.05.046.

ACKNOWLEDGMENTS

We thank Nancy Kleckner (Harvard University) for stimulating discussions, Karlene Cimprich (Stanford University), Oscar F. Capetillo (CNIO) for reagents and suggestions, Gururaj Kidiyoor (IFOM) and Radhakrishnan (MBI-NUS) for assistance, the imaging department of CEN and IFOM for support, and Michele Giannattasio, Dana Branzei, and our groups for discussions. A.K. was supported by a long-term European Molecular Biology Organization fellowship, a Marie Curie Intra-European (under grant agreement 274093) fellowship, and a Fondazione Umberto Veronesi postdoctoral fellowship. This work was supported by grants from Associazione Italiana per la Ricerca sul Cancro, Association for International Cancer Research, Telethon-Italy, CEN-Italy, Ministero dell'Istruzione Universitaria e della Ricerca, the Danish Cancer Society, the Lundbeck Foundation, the Danish Council for Independent Research, and the European Commission (projects DDResponse, aDDRess, Biomedreg). G.V.S. is funded by the Mechanobiology Institute, NUS, Singapore.

Received: November 23, 2013
Revised: April 14, 2014
Accepted: May 28, 2014
Published: July 31, 2014

REFERENCES

Aguilar, P.S., and de Mendoza, D. (2006). Control of fatty acid desaturation: a mechanism conserved from bacteria to humans. Mol. Microbiol. *62*, 1507–1514.

Alderton, G.K., Joenje, H., Varon, R., Børglum, A.D., Jeggo, P.A., and O'Driscoll, M. (2004). Seckel syndrome exhibits cellular features demonstrating defects in the ATR-signalling pathway. Hum. Mol. Genet. *13*, 3127–3138.

Bakkenist, C.J., and Kastan, M.B. (2003). DNA damage activates ATM through intermolecular autophosphorylation and dimer dissociation. Nature *421*, 499–506.

Beaudouin, J., Gerlich, D., Daigle, N., Eils, R., and Ellenberg, J. (2002). Nuclear envelope breakdown proceeds by microtubule-induced tearing of the lamina. Cell *108*, 83–96.

Berchtold, D., Piccolis, M., Chiaruttini, N., Riezman, I., Riezman, H., Roux, A., Walther, T.C., and Loewith, R. (2012). Plasma membrane stress induces relocalization of Slm proteins and activation of TORC2 to promote sphingolipid synthesis. Nat. Cell Biol. *14*, 542–547.

Bermejo, R., Kumar, A., and Foiani, M. (2012a). Preserving the genome by regulating chromatin association with the nuclear envelope. Trends Cell Biol. *22*, 465–473.

Bermejo, R., Lai, M.S., and Foiani, M. (2012b). Preventing replication stress to maintain genome stability: resolving conflicts between replication and transcription. Mol. Cell *45*, 710–718.

Bermejo, R., Doksani, Y., Capra, T., Katou, Y.M., Tanaka, H., Shirahige, K., and Foiani, M. (2007). Top1- and Top2-mediated topological transitions at replication forks ensure fork progression and stability and prevent DNA damage checkpoint activation. Genes Dev. *21*, 1921–1936.

Bermejo, R., Capra, T., Jossen, R., Colosio, A., Frattini, C., Carotenuto, W., Cocito, A., Doksani, Y., Klein, H., Gómez-González, B., et al. (2011). The replication checkpoint protects fork stability by releasing transcribed genes from nuclear pores. Cell *146*, 233–246.

Blasius, M., Forment, J.V., Thakkar, N., Wagner, S.A., Choudhary, C., and Jackson, S.P. (2011). A phospho-proteomic screen identifies substrates of the checkpoint kinase Chk1. Genome Biol. *12*, R78.

Bourgeois, C.A., Hemon, D., and Bouteille, M. (1979). Structural relationship between the nucleolus and the nuclear envelope. J. Ultrastruct. Res. *68*, 328–340.

Brown, E.J., and Baltimore, D. (2003). Essential and dispensable roles of ATR in cell cycle arrest and genome maintenance. Genes Dev. *17*, 615–628.

Casper, A.M., Nghiem, P., Arlt, M.F., and Glover, T.W. (2002). ATR regulates fragile site stability. Cell *111*, 779–789.

Cha, R.S., and Kleckner, N. (2002). ATR homolog Mec1 promotes fork progression, thus averting breaks in replication slow zones. Science *297*, 602–606.

Comings, D.E. (1980). Arrangement of chromatin in the nucleus. Hum. Genet. *53*, 131–143.

Dimitrova, D.S., and Gilbert, D.M. (1999). The spatial position and replication timing of chromosomal domains are both established in early G1 phase. Mol. Cell *4*, 983–993.

Dimitrova, D.S., Todorov, I.T., Melendy, T., and Gilbert, D.M. (1999). Mcm2, but not RPA, is a component of the mammalian early G1-phase prereplication complex. J. Cell Biol. *146*, 709–722.

Duursma, A.M., Driscoll, R., Elias, J.E., and Cimprich, K.A. (2013). A role for the MRN complex in ATR activation via TOPBP1 recruitment. Mol. Cell *50*, 116–122.

Enserink, J.M., Smolka, M.B., Zhou, H., and Kolodner, R.D. (2006). Checkpoint proteins control morphogenetic events during DNA replication stress in Saccharomyces cerevisiae. J. Cell Biol. *175*, 729–741.

Friedl, P., Wolf, K., and Lammerding, J. (2011). Nuclear mechanics during cell migration. Curr. Opin. Cell Biol. *23*, 55–64.

Fujikawa-Yamamoto, K., and Odashima, S. (1989). Effects of hydroxyurea on the phagocytosis of microspheres in V79 cells. Cell Struct. Funct. *14*, 485–493.

Gerlitz, G., and Bustin, M. (2010). Efficient cell migration requires global chromatin condensation. J. Cell Sci. *123*, 2207–2217.

Grinthal, A., Adamovic, I., Weiner, B., Karplus, M., and Kleckner, N. (2010). PR65, the HEAT-repeat scaffold of phosphatase PP2A, is an elastic connector that links force and catalysis. Proc. Natl. Acad. Sci. USA *107*, 2467–2472.

Hashash, N., Johnson, A.L., and Cha, R.S. (2012). Topoisomerase II- and condensin-dependent breakage of MEC1ATR-sensitive fragile sites occurs independently of spindle tension, anaphase, or cytokinesis. PLoS Genet. *8*, e1002978.

Hu, S.H., Chen, J.X., Butler, J.P., and Wang, N. (2005). Prestress mediates force propagation into the nucleus. Biochem. Biophys. Res. Commun. *329*, 423–428.

Jackson, S.P., and Bartek, J. (2009). The DNA-damage response in human biology and disease. Nature *461*, 1071–1078.

Krämer, A., Mailand, N., Lukas, C., Syljuåsen, R.G., Wilkinson, C.J., Nigg, E.A., Bartek, J., and Lukas, J. (2004). Centrosome-associated Chk1 prevents premature activation of cyclin-B-Cdk1 kinase. Nat. Cell Biol. *6*, 884–891.

Kremer, B.E., Adang, L.A., and Macara, I.G. (2007). Septins regulate actin organization and cell-cycle arrest through nuclear accumulation of NCK mediated by SOCS7. Cell *130*, 837–850.

Kudo, N., Wolff, B., Sekimoto, T., Schreiner, E.P., Yoneda, Y., Yanagida, M., Horinouchi, S., and Yoshida, M. (1998). Leptomycin B inhibition of signal-mediated nuclear export by direct binding to CRM1. Exp. Cell Res. *242*, 540–547.

Kültz, D., and Chakravarty, D. (2001). Hyperosmolality in the form of elevated NaCl but not urea causes DNA damage in murine kidney cells. Proc. Natl. Acad. Sci. USA *98*, 1999–2004.

Kumar, A., Marqués, M., and Carrera, A.C. (2006). Phosphoinositide 3-kinase activation in late G1 is required for c-Myc stabilization and S phase entry. Mol. Cell. Biol. *26*, 9116–9125.

Kumar, A., Fernandez-Capetillo, O., and Carrera, A.C. (2010). Nuclear phosphoinositide 3-kinase beta controls double-strand break DNA repair. Proc. Natl. Acad. Sci. USA *107*, 7491–7496.

Kumar, A., Redondo-Muñoz, J., Perez-García, V., Cortes, I., Chagoyen, M., and Carrera, A.C. (2011). Nuclear but not cytosolic phosphoinositide 3-kinase beta has an essential function in cell survival. Mol. Cell. Biol. *31*, 2122–2133.

Kweon, H.S., Beznoussenko, G.V., Micaroni, M., Polishchuk, R.S., Trucco, A., Martella, O., Di Giandomenico, D., Marra, P., Fusella, A., Di Pentima, A., et al. (2004). Golgi enzymes are enriched in perforated zones of golgi cisternae but are depleted in COPI vesicles. Mol. Biol. Cell *15*, 4710–4724.

Mammoto, A., Mammoto, T., and Ingber, D.E. (2012). Mechanosensitive mechanisms in transcriptional regulation. J. Cell Sci. *125*, 3061–3073.

Maniotis, A.J., Chen, C.S., and Ingber, D.E. (1997). Demonstration of mechanical connections between integrins, cytoskeletal filaments, and nucleoplasm that stabilize nuclear structure. Proc. Natl. Acad. Sci. USA *94*, 849–854.

Martins, R.P., Finan, J.D., Guilak, F., and Lee, D.A. (2012). Mechanical regulation of nuclear structure and function. Annu. Rev. Biomed. Eng. *14*, 431–455.

Marqués, M., Kumar, A., Poveda, A.M., Zuluaga, S., Hernandez, C., Jackson, S., Pasero, P., and Carrera, A.C. (2009). Specific function of phosphoinositide 3-kinase beta in the control of DNA replication. Proc. Natl. Acad. Sci. USA *106*, 7525–7530.

Matsuoka, S., Ballif, B.A., Smogorzewska, A., McDonald, E.R., 3rd, Hurov, K.E., Luo, J., Bakalarski, C.E., Zhao, Z., Solimini, N., Lerenthal, Y., et al. (2007). ATM and ATR substrate analysis reveals extensive protein networks responsive to DNA damage. Science *316*, 1160–1166.

Mazumder, A., Roopa, T., Basu, A., Mahadevan, L., and Shivashankar, G.V. (2008). Dynamics of chromatin decondensation reveals the structural integrity of a mechanically prestressed nucleus. Biophys. J. *95*, 3028–3035.

McMahon, H.T., and Gallop, J.L. (2005). Membrane curvature and mechanisms of dynamic cell membrane remodelling. Nature *438*, 590–596.

Mekhail, K., and Moazed, D. (2010). The nuclear envelope in genome organization, expression and stability. Nat. Rev. Mol. Cell Biol. *11*, 317–328.

Mironov, A.A., and Beznoussenko, G.V. (2009). Correlative microscopy: a potent tool for the study of rare or unique cellular and tissue events. J. Microsc. *235*, 308–321.

Mironov, A.A., and Beznoussenko, G.V. (2012). Correlative light-electron microscopy a potent tool for the imaging of rare or unique cellular and tissue events and structures. Methods Enzymol. *504*, 201–219.

Murga, M., Bunting, S., Montaña, M.F., Soria, R., Mulero, F., Cañamero, M., Lee, Y., McKinnon, P.J., Nussenzweig, A., and Fernandez-Capetillo, O. (2009). A mouse model of ATR-Seckel shows embryonic replicative stress and accelerated aging. Nat. Genet. *41*, 891–898.

Nghiem, P., Park, P.K., Kim, Y., Vaziri, C., and Schreiber, S.L. (2001). ATR inhibition selectively sensitizes G1 checkpoint-deficient cells to lethal premature chromatin condensation. Proc. Natl. Acad. Sci. USA *98*, 9092–9097.

O'Driscoll, M., Ruiz-Perez, V.L., Woods, C.G., Jeggo, P.A., and Goodship, J.A. (2003). A splicing mutation affecting expression of ataxia-telangiectasia and Rad3-related protein (ATR) results in Seckel syndrome. Nat. Genet. *33*, 497–501.

Ostlund, C., Sullivan, T., Stewart, C.L., and Worman, H.J. (2006). Dependence of diffusional mobility of integral inner nuclear membrane proteins on A-type lamins. Biochemistry *45*, 1374–1382.

Perry, J., and Kleckner, N. (2003). The ATRs, ATMs, and TORs are giant HEAT repeat proteins. Cell *112*, 151–155.

Polishchuk, R.S., Polishchuk, E.V., and Mironov, A.A. (1999). Coalescence of Golgi fragments in microtubule-deprived living cells. Eur. J. Cell Biol. *78*, 170–185.

Rowat, A.C., Lammerding, J., and Ipsen, J.H. (2006). Mechanical properties of the cell nucleus and the effect of emerin deficiency. Biophys. J. *91*, 4649–4664.

Shevelyov, Y.Y., and Nurminsky, D.I. (2012). The nuclear lamina as a gene-silencing hub. Curr. Issues Mol. Biol. *14*, 27–38.

Shivashankar, G.V. (2011). Mechanosignaling to the cell nucleus and gene regulation. Annu. Rev. Biophys. *40*, 361–378.

Simon, D.N., and Wilson, K.L. (2011). The nucleoskeleton as a genome-associated dynamic 'network of networks'. Nat. Rev. Mol. Cell Biol. *12*, 695–708.

Sogo, J.M., Lopes, M., and Foiani, M. (2002). Fork reversal and ssDNA accumulation at stalled replication forks owing to checkpoint defects. Science *297*, 599–602.

Tibbetts, R.S., Cortez, D., Brumbaugh, K.M., Scully, R., Livingston, D., Elledge, S.J., and Abraham, R.T. (2000). Functional interactions between BRCA1 and

the checkpoint kinase ATR during genotoxic stress. Genes Dev. *14*, 2989–3002.

Toledo, L.I., Murga, M., Zur, R., Soria, R., Rodriguez, A., Martinez, S., Oyarzabal, J., Pastor, J., Bischoff, J.R., and Fernandez-Capetillo, O. (2011). A cell-based screen identifies ATR inhibitors with synthetic lethal properties for cancer-associated mutations. Nat. Struct. Mol. Biol. *18*, 721–727.

Toledo, L.I., Altmeyer, M., Rask, M.B., Lukas, C., Larsen, D.H., Povlsen, L.K., Bekker- Jensen, S., Mailand, N., Bartek, J., and Lukas, J. (2013). ATR prohibits replication catastrophe by preventing global exhaustion of RPA. Cell *155*, 1088–1103.

Towbin, B.D., Meister, P., and Gasser, S.M. (2009). The nuclear envelope—a scaffold for silencing? Curr. Opin. Genet. Dev. *19*, 180–186.

Vassin, V.M., Anantha, R.W., Sokolova, E., Kanner, S., and Borowiec, J.A. (2009). Human RPA phosphorylation by ATR stimulates DNA synthesis and prevents ssDNA accumulation during DNA-replication stress. J. Cell Sci. *122*, 4070–4080.

Vigh, L., Nakamoto, H., Landry, J., Gomez-Munoz, A., Harwood, J.L., and Horvath, I. (2007). Membrane regulation of the stress response from prokaryotic models to mammalian cells. Ann. N Y Acad. Sci. *1113*, 40–51.

Wang, J.C. (2002). Cellular roles of DNA topoisomerases: a molecular perspective. Nat. Rev. Mol. Cell Biol. *3*, 430–440.

Wang, N., Tytell, J.D., and Ingber, D.E. (2009). Mechanotransduction at a distance: mechanically coupling the extracellular matrix with the nucleus. Nat. Rev. Mol. Cell Biol. *10*, 75–82.

Wang, X., Zou, L., Lu, T., Bao, S., Hurov, K.E., Hittelman, W.N., Elledge, S.J., and Li, L. (2006). Rad17 phosphorylation is required for claspin recruitment and Chk1 activation in response to replication stress. Mol. Cell *23*, 331–341.

Wilsker, D., Petermann, E., Helleday, T., and Bunz, F. (2008). Essential function of Chk1 can be uncoupled from DNA damage checkpoint and replication control. Proc. Natl. Acad. Sci. USA *105*, 20752–20757.

Wolf, K., and Friedl, P. (2009). Mapping proteolytic cancer cell-extracellular matrix interfaces. Clin. Exp. Metastasis *26*, 289–298.

Zhang, S., Hemmerich, P., and Grosse, F. (2007a). Centrosomal localization of DNA damage checkpoint proteins. J. Cell. Biochem. *101*, 451–465.

Zhang, X.H., Zhao, C., and Ma, Z.A. (2007b). The increase of cell-membranous phosphatidylcholines containing polyunsaturated fatty acid residues induces phosphorylation of p53 through activation of ATR. J. Cell Sci. *120*, 4134–4143.

Zou, L., and Elledge, S.J. (2003). Sensing DNA damage through ATRIP recognition of RPA-ssDNA complexes. Science *300*, 1542–1548.

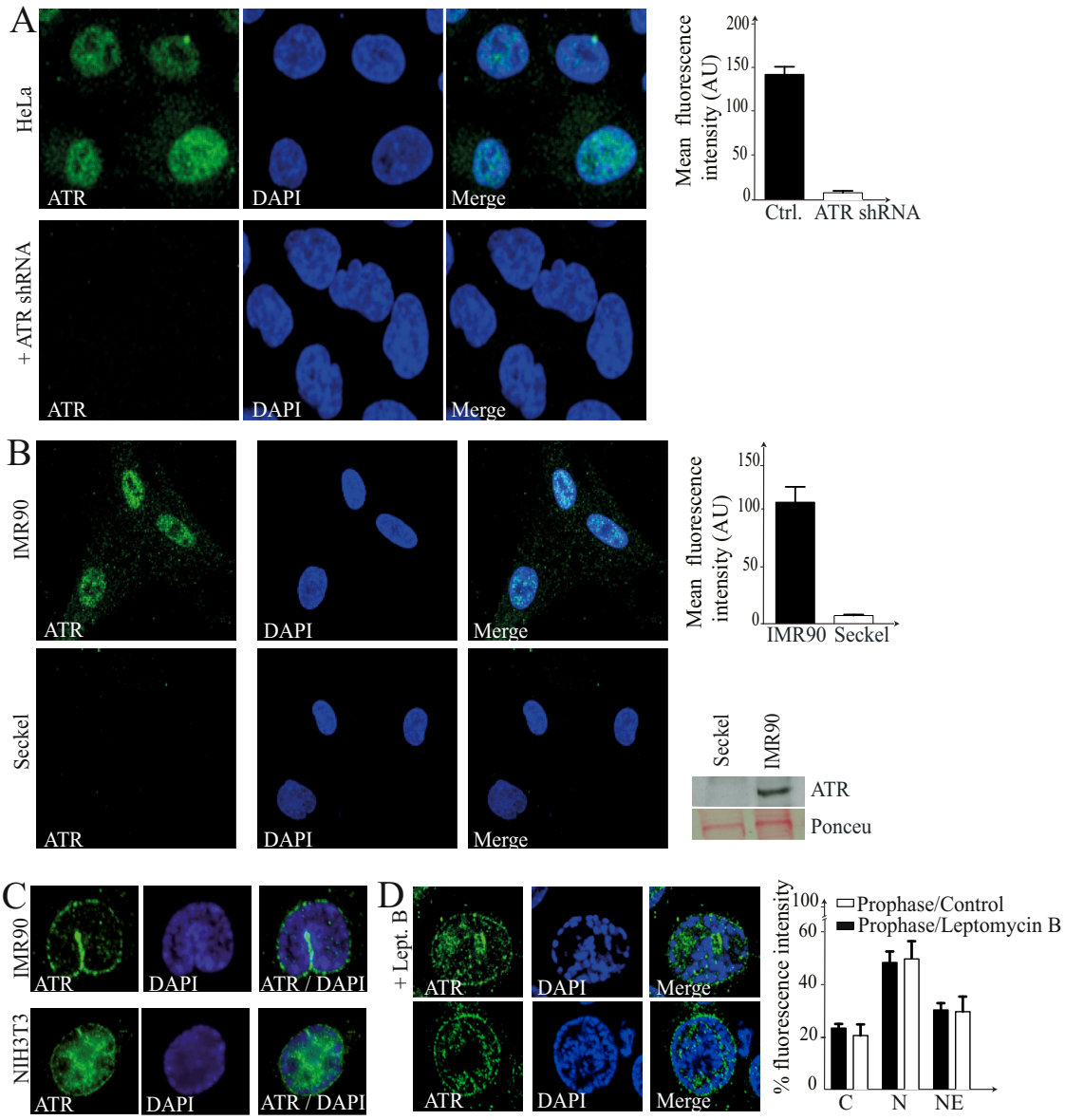

Figure S1. Prophase-Specific Nuclear Envelope Localization of ATR during the Cell Cycle, Related to Figure 1

(A) HeLa cells were transfected with vector or ATRshRNA, and selected with 3 μg/ml puromycin (94h) posttransfection, and processed for immunofluorescence using anti-ATR (green), DAPI (blue). Graphs show the mean fluorescence intensity on a representative set of cells (n = 20).

(B) IMR90 or human primary Seckel cells containing hypomorphic mutation in ATR, were fixed and processed for IF using anti-ATR (green), DAPI (blue). Graphs show the mean fluorescence intensity on a representative set of cells (n = 20); (lower right panel) western blot analysis of cell lysates from IMR90 and Seckel cells using ATR ab. Ponceu staining was used as loading control.

(C) IMR90 and NIH 3T3 cells in prophase were stained for ATR (green) and DAPI (blue).

(D) HeLa cells were either treated mock or with nuclear export inhibitor Laptomycin B (10 nM) for 2hrs. and processed for immunofluorescence using anti-ATR (green), DAPI (blue). The images depict prophase cell stained with ATR in presence or absence of Leptomycin B (Lept. B). Graphs show %- fluorescence intensity on a representative set of cells (n = 10). IF images show single optical sections of cells stained with ATR Ab.

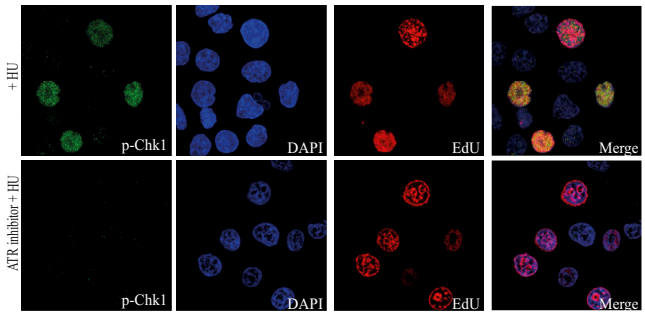

Figure S2. Specificity of Chk1-phospho-S345 Ab, Related to Figure 2

HeLa cells were incubated with or without ATR specific inhibitor (2 μM; 2hr) followed by addition of Hydroxyurea (5 mM; 1h) to induce replication stress and stained with anti-p-Chk1 Ab and DAPI. A representative image of n = 20 is shown.

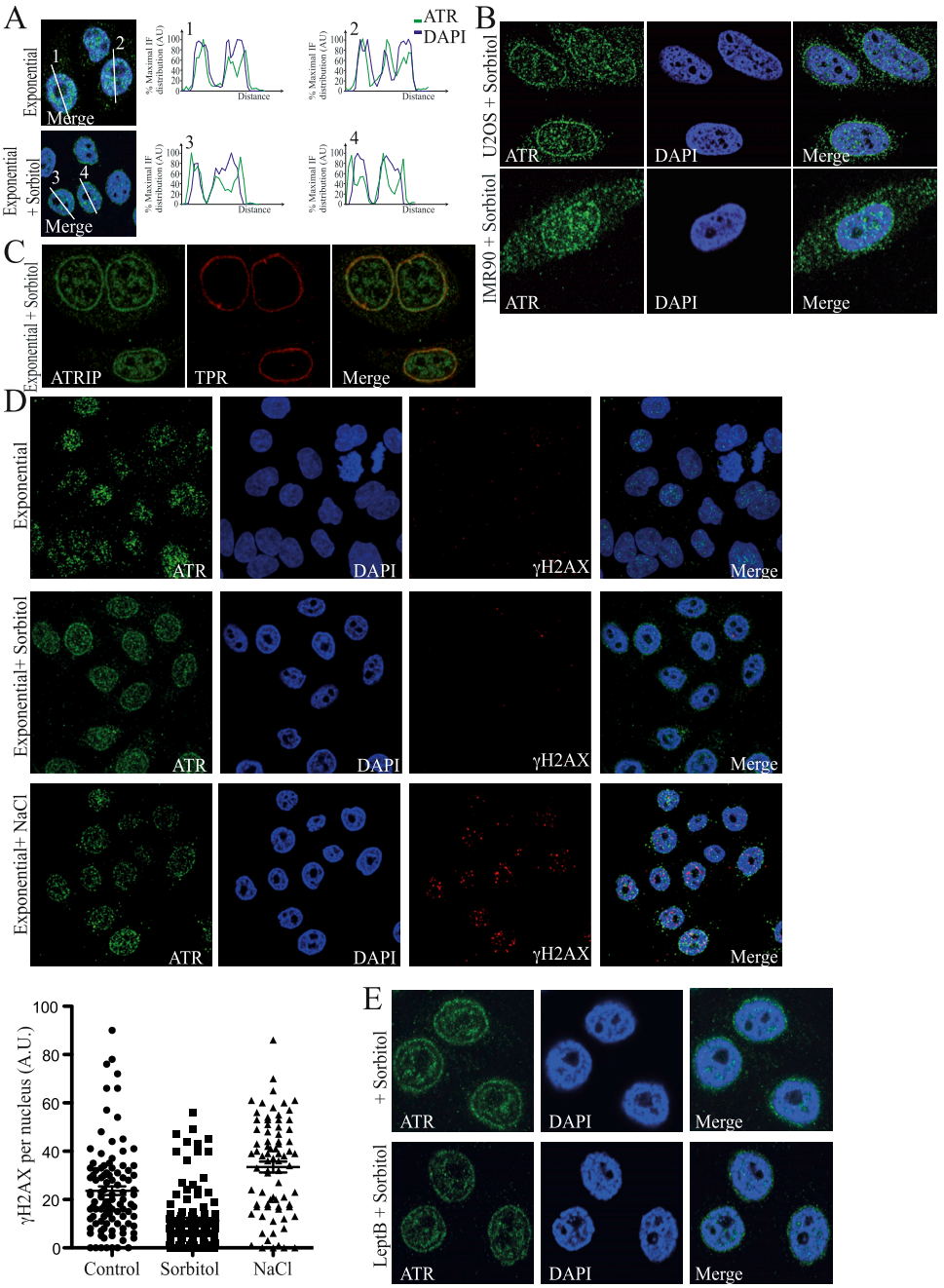

Figure S3. Osmotic Stress Induces ATR Activation and Nuclear Envelope Relocalization, Related to Figure 3

(A) Redistribution of ATR and chromatin in response to osmotic stress. The analysis was carried out on the merged images in Figure 3B. The graphs illustrate the quantification in arbitrary units (AU) of the distribution of ATR and DAPI by IF along the lines (highlighted by numbers) shown in the merged panels.

(B) U2OS and IMR90 cells were treated with hypertonic medium and after 20 min. cells were processed for immuno-fluorescence using anti-ATR (green) and DAPI (blue).

(C) Exponentially growing HeLa cells were treated with hypertonic medium (0.5 M Sorbitol; 20-30 min.) and stained with ATRIP (green), DAPI (blue) and nucleoporin TPR.

(D) HeLa cells were maintained in isotonic medium, hypertonic medium containing either 0.5 M sorbitol or 0.4 M NaCl for 20 min. Cells were stained with anti-ATR (green), DAPI (blue) and γH2AX to visualize DNA damage. IF images show single optical sections of cells stained with corresponding Ab. Graphs show the number of foci with signal intensity higher than the basal γ−H2AX levels observed (bottom panel) on a representative set of cells (n > 75).

(E) HeLa cells were either mock treated or with nuclear export inhibitor Laptomycin B (10 nM; 2hrs.) followed by treatment with hypertonic medium (0.5 M Sorbitol; 20-30 min.) and stained with ATR (green), DAPI (blue). The samples were processed for immunofluorescence using anti-ATR (green), DAPI (blue).

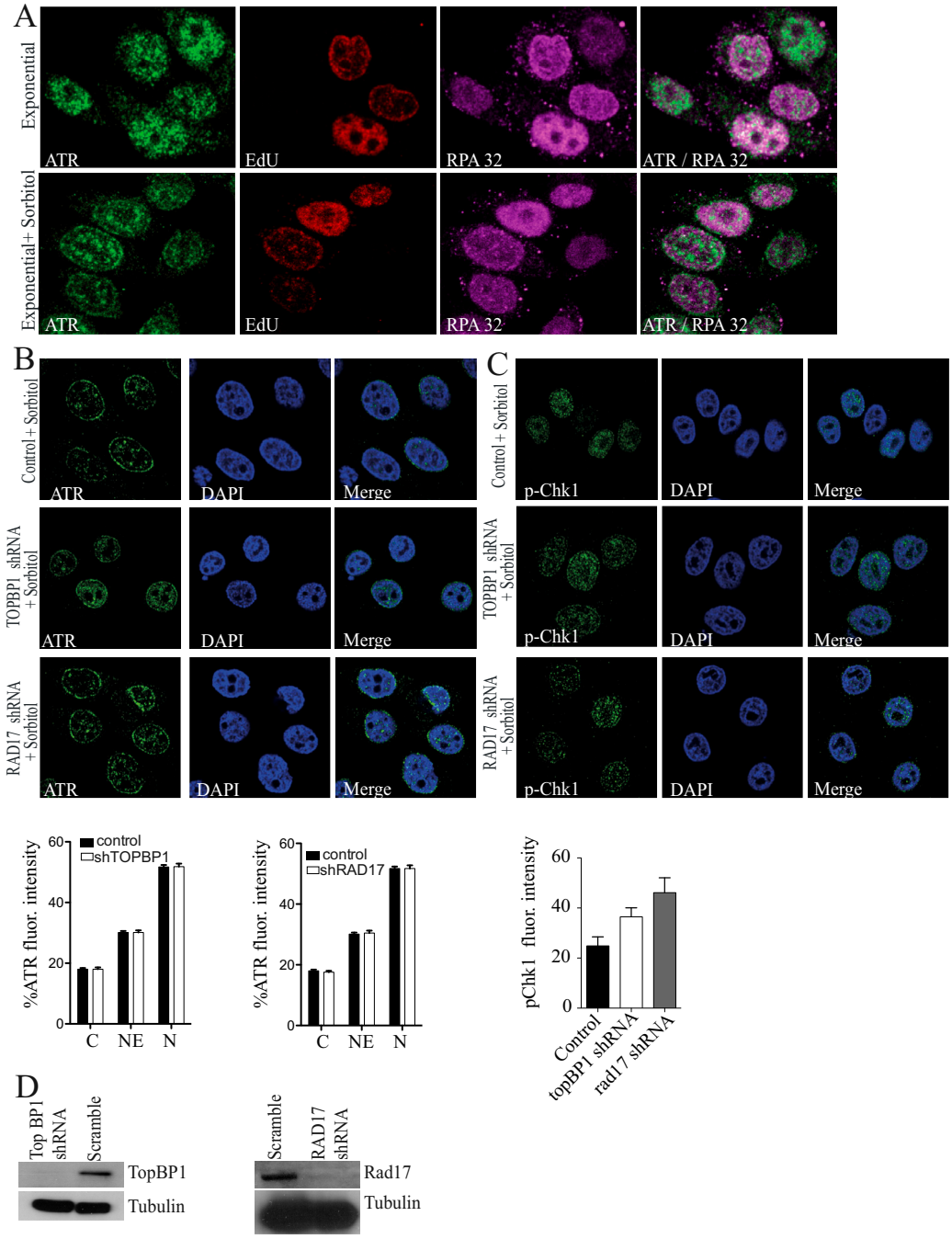

Figure S4. ATR Nuclear Envelope Translocation and Activation following Osmotic Stress Is TOPBP1 and RAD17 Independent, Related to Figure 4

(A) Images of exponentially growing HeLa cells maintained in either normal or hypertonic medium (0.5 M Sorbitol; 20 min.). Cells were stained with anti-ATR (green), S-phase specific EdU (red), RPA32 (magenta) and DAPI (blue).

(B and C) HeLa cells were transfected with empty-vector, TOPBP1 shRNA or RAD17 shRNA and selected with 3 μg/ml puromycin (72h). HeLa cells were incubated with hypertonic medium containing 0.5 M sorbitol for 20 min and stained with ATR/p-Chk1 (green), and DAPI (blue). TOPBP1 and RAD17 protein levels were analyzed by western blot using anti-TOPBP1 Ab or anti-RAD17 Ab and anti-tubulin as loading control (lower panel). Graphs show the % ATR fluorescence intensity in different cell compartments on a representative set of cells (n = 15) and p-Chk1 fluorescence intensity on a representative set of cells (n = 20) respectively.

(D) Western blots showing RAD17, TOPBP1 protein levels, following transfection of HeLa cells with empy-vector, *TOPBP1* shRNA or *RAD17* shRNA, respectively, and selection with 3μg/ml puromycin (72h) posttransfection. Anti- tubulin Ab was used as loading control.

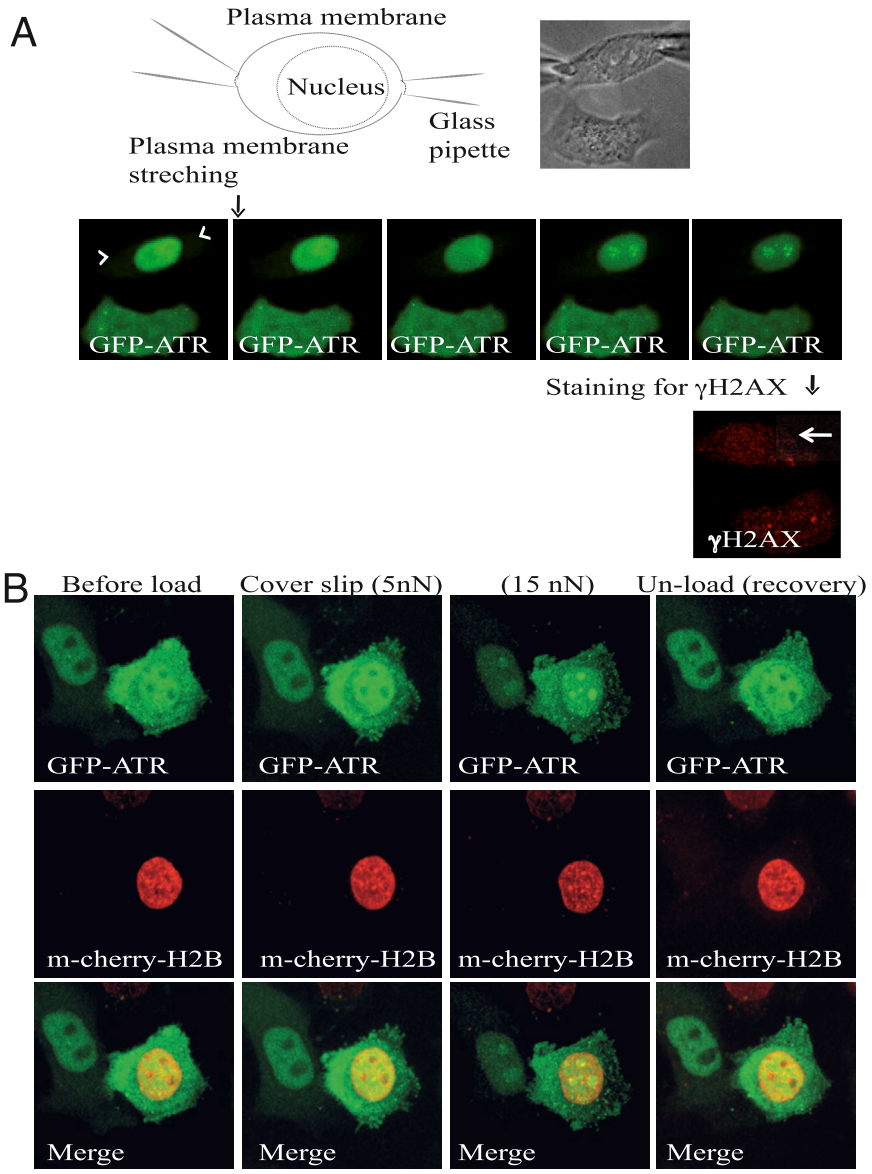

Figure S5. The ATR Response to Cells Stretching and Compression Is DNA Damage Independent and Reversible, Related to Figure 5

(A) Schematic representation of two-patch clamp pipettes positioned on the two opposite sides of the plasma membrane. The corresponding microscope image is on the right. The white arrows indicate the points of focal tension induced by the mechanical stretching. Two patch pipettes were attached to the plasma membrane of a HeLa cell expressing GFP-ATR (green) and stretched to induce mechanical stress on the membranes. The intracellular changes in GFP-ATR localization was examined in real-time with a gap of 30 s. The cells were fixed using 4% formadehyde and later stained for γH2X to examine the DNA damage state in the cell of interest.

(B) HeLa cells coexpressing GFP-ATR (green), mCherry-H2B (red) were compressed with 30nN force using weights and the intracellular changes in GFP-ATR localization and chromatin architecture (m-cherry H2B) was examined with a gap of 10 min. Later the weights were removed to withdraw the forces exerted on the cells and again intracellular changes in GFP-ATR localization and chromatin architecture (m-cherry H2B) were recorded (after 7 min of weight removal) to examine the reversal in the ATR response and chromatin state.

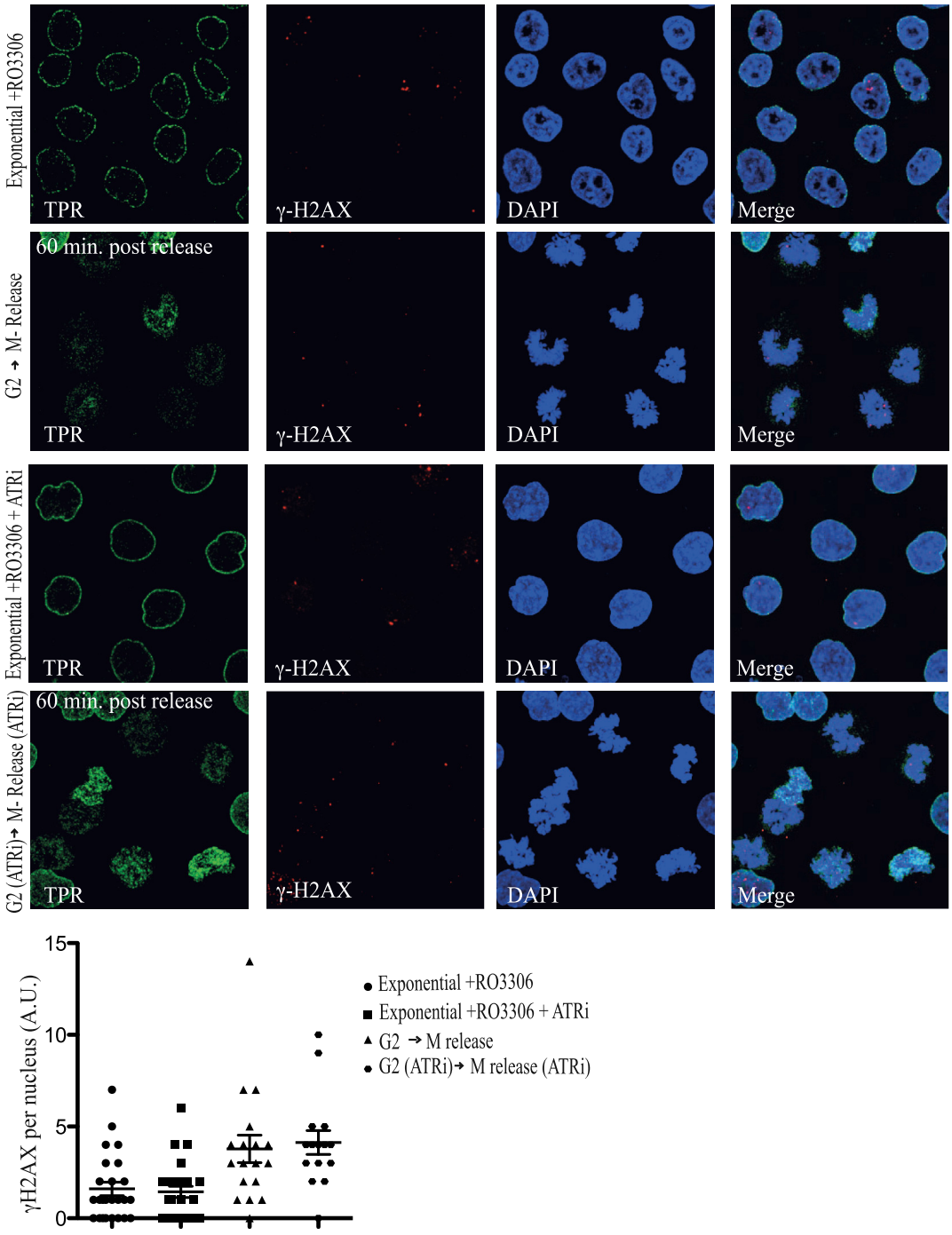

Figure S6. ATR Inhibition in G2/M Does Not Cause Accumulation of γ-H2AX, Related to Figure 6

R3306 Cdk1 inhibitor (10 μM, 16 hr.) was used to arrest HeLa cells in G2, followed by incubation with DMSO or ATR inhibitor (3 μM, 1hr). The cells were then released into mitosis (for 60 min) ± ATRi. Cells were stained with anti-TPR (green), γ-H2AX (red) to visualize DNA damage, and DAPI (blue). Quantification of γ-H2AX is shown.